Universitat de les Illes Balears

CSIC UIB

IFISC

Instituto de Física Interdisciplinar y Sistemas Complejos

DOCTORAL THESIS

2015

COMPLEX DYNAMICS IN PHOTONIC DELAY SYSTEMS: A STORY OF CONSISTENCY AND UNPREDICTABILITY

Neus Oliver Andreu

Universitat de les Illes Balears

Instituto de Física Interdisciplinar y Sistemas Complejos

DOCTORAL THESIS
2015

Doctoral Program of Physics

COMPLEX DYNAMICS OF PHOTONIC DELAY SYSTEMS: A STORY OF CONSISTENCY AND UNPREDICTABILITY

Neus Oliver Andreu

Thesis Supervisor: Ingo Fischer

Tutor: Claudio R. Mirasso

Doctor by the Universitat de les Illes Balears

Complex dynamics in photonic delay systems: a story of consistency and unpredictability

Neus Oliver Andreu
Tesis presentada en el Departamento de Física de la Universitat de les Illes Balears

PhD Thesis

Director: Dr. Ingo Fischer

El Profesor Ingo Fischer, Profesor de Investigación del Consejo Superior de Investigaciones Científicas (CSIC) y el Profesor Claudio Mirasso, Catedrático de Universidad (UIB),

HACEN CONSTAR

que esta tesis doctoral ha sido realizada por la Sra. *Neus Oliver Andreu* bajo su dirección en el Instituto de Física Interdisciplinar y Sistemes Complejos (UIB-CSIC) y, para dejar constancia, firma la misma.

Palma, 12 de noviembre de 2015

Ingo Fischer
Director

Claudio Mirasso
Ponente

Neus Oliver Andreu
Doctorando

When you come out of the storm you won't be the same person that walked in. That's what the storm is all about. - Haruki Murakami.

Resumen

El campo de la fotónica está revolucionado nuestra industria y sociedad actuales. Sus usos no se limitan a ciencia avanzada y muchas de sus aplicaciones están integradas en nuestra vida diaria: internet depende de las comunicaciones ópticas por fibra, los láseres son una herramienta más en cirujía médica y fabricación industrial, y el uso de la luz ha facilitado el desarrollo de técnicas de metrología, entre otros.

La fenomenología en fotónica hace de ella un campo lleno de posibilidades y potencial por explorar. Dos de las áreas más prometedoras son el procesamiento de información y comunicaciones ópticas seguras. Contribuyendo a dichas áreas, esta tesis estudia el comportamiento complejo y emergente en un sistema fotónico concreto: el láser de semiconductor con retroalimentación. Este sencillo sistema es capaz de generar gran variedad de regímenes dinámicos, como caos determinista. Con él, abarcamos las propiedades de consistencia para el procesamiento de la información, y la generación de números aleatorios, escribiendo una historia de consistencia e impredecibilidad.

Sobre consistencia o cómo procesar información por medios fotónicos

Nuestro cerebro es un órgano eficiente, capaz de realizar de manera fiable tareas complicadas como el reconocimiento de caras. Inspirándose en el cerebro, se han desarrollado nuevos métodos para imitar el procesamiento de la información en redes neuronales, entre ellos "Reservoir Computing". En esta técnica, un sistema fotónico no lineal es capaz de efectuar tareas computacionalmente arduas al proporcionar respuestas consistentes a señales de entrada.

La capacidad de un sistema de responder de manera similar a estímulos similares, o consistencia, es una cualidad natural que, sorprendentemente, no está asegurada. Su cuantificación y mecanismos causantes son temas por investigar y los láseres de semiconductor con retroalimentación representan una plataforma excelente para ello.

Por medio de tres experimentos investigamos, caracterizamos y cuantificamos las propiedades de consistencia en esquemas ópticos y optoelectrónicos. Los experimentos ilustran transiciones entre respuestas consistentes e inconsistentes, así como su dependencia con respecto al tipo y naturaleza de la señal de entrada. Más allá del mundo de la fotónica, la consistencia es un concepto relevante en ciencia y tecnología. Las propiedades y métodos desarrollados en esta tesis representan un avance para futuras investigaciones y aplicaciones.

Sobre impredecibilidad o cómo implementar un generador de números aleatorios óptico

Los números (bits) aleatorios, son cruciales para transmisión de información segura, juegos online, simulaciones numéricas o criptografía. Su ubicuidad ha provocado la aparición de generadores de números aleatorios (RNGs) basados en componentes fotónicos con claras ventajas: pueden integrarse fácilmente en sistemas de telecomunicaciones actuales y permiten la generación a velocidades altas (Gbit/s). Aunque se han implementado algunos RNGs ópticos exitósamente, quedan cuestiones por resolver: ¿Es posible emplear esquemas más sencillos para generar números aleatorios? ¿Estamos empleando los RNGs de manera óptima? ¿Cuál es el ritmo máximo de generación posible? ¿Podemos conocerlo de antemano? Esta tesis contribuye a responderlas. Proponemos un experimento simple basado en un láser de semiconductor con retroalimentación, aprovechando la impredecibilidad de su dinámica caótica. Sin embargo, la dinámica es condición necesaria pero no suficiente para obtener números aleatorios. En la comprensión de los factores determinantes en la generación de números aleatorios y las altas velocidades de generación reside la relevancia de este trabajo.

Summary

The field of photonics is revolutionizing the current industry and society, analogously to what electronics did during the 20th century. The uses of photonics seem endless and are not restricted to advanced science. Some of its applications have already become mature technologies, and belong now to our everyday life: internet relies on optical fiber communications, lasers are an integrated tool in medical surgery and industrial manufacturing, and the use of light has facilitated the measurement techniques in metrology, among many others.

The rich phenomenology in photonics makes it an emerging field with open perspectives, whose full capabilities are still to be exploited. Specifically, two of the promising areas for photonics are information processing and secure optical communications. Complex phenomena in photonics can serve as a backbone for both applications. This Thesis comprises the study of the emerging complex behavior in a concrete photonic system: a semiconductor laser with delayed feedback. This simple system can generate an interesting variety of dynamical regimes, like deterministic chaos and, therefore, we use it to contribute to the above mentioned areas. More precisely, we address the consistency properties for bio-inspired photonic information processing and the optical generation of random numbers, thereby telling a story of consistency and unpredictability.

On consistency or how to perform reliably photonic information processing

Our brain is a fast and efficient organ, capable of performing reliably tasks that for any computer would be rather hard, such as face recognition. Inspired by our brain, technical systems have been introduced to mimic information processing in neural networks. Understanding how these systems process information can lead to faster, low-energy demanding computing. A recent technique for photonic information processing is Reservoir Computing. In Reservoir Computing, a nonlinear system performs computationally hard tasks, like spoken digit recognition. Its operation is based on providing a consistent nonlinear response with respect to an input signal, exactly as neurons do: they respond reliably to electrical and chemical signals when processing information.

Consistency, as the ability of the system to respond in a similar way to similar inputs, is therefore a key-ingredient to be studied. Surprisingly, consistency in nature is not always a given, and a system might change from a consistent response to an inconsistent one. The mechanisms underlying consistency as well as its quantification are thus pertinent proper questions. Semiconductor lasers with feedback represent again an excellent platform for its investigation.

We approach these aspects by designing three experiments to investigate and characterize the consistency properties of semiconductor laser with delayed optical and opto-electronic feedback. The high quality of the experiments allow us to illustrate the occurrence of transitions between consistent and inconsistent responses in the laser, and characterize their dependence on the drive signal. Thus, we utilize various drive signals, both optical and electrical, and present different ways to quantify consistency, including correlations and a direct measure for the sub-Lyapunov exponent. Beyond photonics, consistency in driven systems is a fundamental and far-reaching concept, present in nature and technology. Therefore, the fundamental properties and the developed method represent valuable findings for further fundamental investigations and applications.

On unpredictability or how to implement an optical random number generator

Random numbers (or random bits) are crucial for information security, online-gaming, complex numerical simulations and cryptography. Their ubiquity has led to the emergence of random number generators (RNGs) based on photonic components, given the intrinsic advantages of photonics: first, an optical RNG is easy to integrate into telecommunication systems; and second, a photonic approach to random number generation allows for high generation speeds of order of gigabits per second (Gbit/s), a key demand of current random number generators. Although some optical approaches to random bit generation had been successfully put forward, open questions still remained: Is it possible to employ simpler schemes to generate random numbers? Are we using the RNG optimally or can its performance be enhanced? What is the maximum bit rate attainable with a given RNG? Can we know it in advance? In this Thesis, we contribute significantly to answer these questions. We propose a strikingly simple experimental setup based on a single semiconductor laser with optical feedback, benefiting from the unpredictability and randomness of the chaotic output of the laser. Nevertheless, chaotic dynamics is only a necessary but not a sufficient condition to obtain random numbers. We present guidelines on the interplay between dynamics, acquisition procedures and post-processing, and predict the potential of any RNG by using Information Theory to estimate the maximum achievable bit rate.

The relevance of this work relies not only on the high speed of the bit rate, up to 160Gbit/s, but also on the understanding of the factors involved in the random bit generation process to guarantee the optimal operation of any laser-based generator.

Acknowledgements

If someone had told me ten years ago that I would be writing these lines today, I wouldn't had believed them. At that time I was convinced that Physics was cool, but not for me. And here I am with a PhD Thesis that has my name on it. Certainly, I could not have done this work without the help and contribution of so many people throughout these years.

I would like to express my deep gratitude to Prof. Ingo Fischer. His patience, support, respect, perseverance, passion towards science and motivation were the constant attributes of his wise guidance. Discussions with him were always a source of inspiration, and despite my atelophobia, he kept encouraging me every time I felt hopeless. From him, I learnt that failure is only part of success and that giving up is never a choice. I feel very lucky to have had as an advisor a person I admire so much, as a scientist and as a human being.

I cannot forget the person responsible of my first steps into research and the first to believe I was capable of pursuing a PhD: Prof. Maxi San Miguel. Thanks for trusting in me. I am also very grateful to Prof. Claudio Mirasso for his advice and for being so supportive and caring during these years. With the doors of his office wide open at any time, he always had encouraging words for me and I can never thank him enough for his kindheartedness.

I would also like to thank all the collaborators and colleagues that I got to meet and from whom I learnt so much: Dr. Miguel C. Soriano for guiding me into the world of experimental photonics, Dr. David Sukow for his kindness, constant support and pleasant emails, Dr. Fan-Yi Lin for his hospitality when I did the research training in Taiwan and Dr. Laurent Larger for welcoming me in his labs and introducing me to the optoelectronic oscillator. I also thank Dr. Daniel Brunner for his willingness to help at any time and always with a smile on his face. I also want to give credit to Dr. Thomas Jüngling. His mentoring, excellent work and, above all, friendship, have meant a lot to me. I also want to thank Dr. Jordi García-Ojalvo, Antonio Pons, Javier Buldú, Maria del Carme Torrent and Jordi Tiana-Alsina.

I am also grateful to each and every person at IFISC, for the inspiring atmosphere they create and the good memories that I will take with me. I am particularly thankful to all the members of the Nonlinear Photonics Lab, specially to my dudes Xavier Porte and Konstantin Hicke. I also want to thank Dr. Pere Colet and Dr. Roberta Zambrini for the nice interactions along these years, and all the current and former students at the S07. I want to express my gratitude to the technical and administrative staff: Marta Ozonas, Inma Carbonell, Rosa María Rodríguez, Rosa Campomar, Rubén Tolosa, Edu Herraiz, Antònia Tugores, Pep Canyelles, Daniel Palou and Edu Solivellas.

As a PhD student I got to meet a lot of amazing colleagues from around the globe. I

am thankful to all the nice people at the National Tsing Hua University in Taiwan, specially Chih-Hao Cheng, Jack Wu and Yi-Huan Liao. To all the scientists I met at FEMTO-ST, particularly to Jacques Chrétien, Bicky A. Márquez, Guoping Lin, Shanti Toenger, Antonio Baylon, Xavier Romain, Tintu Kuriakose, Bogdan Penkovsky and Ignacio Zaldivar. I would also like to mention Dr. Anbang Wang, Dr. Yun-cai Wang and Dr. Alan Shore for the nice time in China.

The best thing about this time as PhD student is to have had colleagues that ended up being real friends. I am happy to have shared so many good times with Marina Diakonova, Antònia Tugores and Thomas Jüngling. Thank you for being by my side and for accepting my craziness with no judgements. I look forward to our next adventures together. I am also deeply grateful to Valérie Moliere, for her tremendous support in my joys and struggles. To my friend Tawnee Hensel, because even though we don't see each other as much as we would like to, we still can count on each other.

Last but not least, I want to thank my parents and my brother. Aunque no seamos la familia más convencional, soy muy feliz de teneros a mi lado. Gracias por apoyarme aún sin saber muy bien qué he estado haciendo. And above all, I want to thank Toni Buades, for being a partner, a friend and a fellow traveler; for his patience, limitless understanding, and for embracing the mess that I am. Thanks for sharing your life with me.

List of Publications

- Neus Oliver, Miguel C. Soriano, David W. Sukow and Ingo Fischer. *Dynamics of a semiconductor laser with polarization-rotated feedback and its utilization for random bit generation.* Optics Letters, **36**, 23, 4632, (2011).
- Neus Oliver, Miguel C. Soriano, David W. Sukow and Ingo Fischer. *Fast random bit generation using a chaotic laser: approaching the information theoretic limit.* Journal of Quantum Electronics, **49**, 11, 910, (2013).
- Neus Oliver, Thomas Jüngling and Ingo Fischer. *Consistency properties of a chaotic semiconductor laser driven by optical feedback.* Physical Review Letters, **114**, 12, 123902, (2015).

Manuscripts in preparation

- Neus Oliver, Javier M. Buldú, Antonio J. Pons, Jordi Tiana-Alsina, M. Carme Torrent, Ingo Fischer and Jordi García-Ojalvo. *Consistency through transient dynamics.* To be submitted, PNAS.
- Neus Oliver, Bicky A. Márquez, Laurent Larger and Ingo Fischer *Forms of consistency in a multistable driven system: the Ikeda oscillator case.*

Conference contributions

- M. C. Soriano, N. Oliver, X. Porte, R. Vicente, I. Fischer and C. R. Mirasso. *Delay Coupled Semiconductor Lasers: Dynamics and Applications.* VII Reunin Iberoamericana de ptica (RIAO). X Encuentro Latinoamericano de ptica, Lseres y Aplicaciones (OPTILAS), Lima, Peru, 2010. **Invited Talk**.
- N. Oliver, M. C. Soriano, D. W. Sukow and I. Fischer. *Dynamics of semiconductor lasers with polarization rotated feedback and its applications for fast random bit generation.* European Conference on Lasers and ElectroOptics (CLEO Europe) and the XIIth European Quantum Electronics Conference, Munich, Germany, 2011. **Talk**.
- N. Oliver, M. C. Soriano, D. W. Sukow and I. Fischer. *Dynamics of semiconductor lasers with delayed polarization rotated feedback and its applications for fast random bit generation.* Combined DPG Spring Meeting, Berlin, Germany, 2012. **Talk**.

- N. Oliver, M. C. Soriano, D. W. Sukow and I. Fischer. *Dynamics of semiconductor lasers with delayed feedback and its applications for fast random bit generation.* International Conference on Delayed Complex Systems (DCS12), Palma de Mallorca, Spain, 2012. **Poster**.

- N. Oliver, M. C. Soriano, D. W. Sukow and I. Fischer. *Experimental Criteria for high-speed random bit generation using a chaotic semiconductor laser.* European Conference on Lasers and Electro-Optics (CLEO Europe) and the XIIIth European Quantum Electronics Conference, Munich, Germany, 2013. **Talk**.

- N. Oliver and I. Fischer. *Exploring chaotic semiconductor lasers for high speed random bit generation: practical and information theoretic limitations.* The 6th International Workshop on Chaos Fractals Theories and Applications, Shanxi, China, 2013. **Invited Keynote**.

- N. Oliver, T. Jüngling, D. Brunner, A. J. Pons, J. Tiana-Alsina, J. Buldú, M. C. Torrent, J. García-Ojalvo and I. Fischer. *Consistency Properties of a Chaotic Laser to Input Pulse Trains.* European Conference on Lasers and Electro-Optics and the European Quantum Electronics Conference, Munich, Germany, 2015. **Poster**.

Contents

CHAPTER 1

Introduction

> It doesn't matter how beautiful your theory is, it doesn't matter how smart you are. If it doesn't agree with experiment, it's wrong.
>
> Richard P. Feynman, Physicist.

In this Thesis, and as its title suggests, the complex dynamics originating from photonic delay systems is explored, putting special emphasis on two emerging properties: consistency and unpredictability.

Semiconductor lasers with delayed feedback are employed to exemplify how a nonlinear system can display these two features. The property of consistency describes the ability of a system to produce complex but still reproducible dynamics in response to a repeated input. This definition already reveals the necessity of a drive-response scheme, in which the laser with delayed feedback acts as the response system. A consistent behavior, when similar drive signals lead to similar outputs, can thus be seen as predictable. Nevertheless, semiconductor laser systems with delay are known to exhibit complex phenomena such as deterministic chaos, with randomness-like features that makes the dynamics unpredictable. These two opposed properties, consistency and unpredictability, can be achieved with robustness in such systems by just tuning the laser parameters, and their controllability enriches even more the variety of current applications of photonic delay systems. Consistency is of key importance for the understanding and harnessing of any implementation of information processing, while unpredictability is the foundation for any cryptographic application.

Consistency is investigated through the analysis of the responses from three different laser systems with delay subjected to a drive. The transitions between inconsistent and consistent behavior as a function of parameters is illustrated, and different methods to evaluate the degree of consistency are introduced. The property of unpredictability is also studied by means of a semiconductor laser with delayed feedback, only that here, no input signals are used. Tailoring the optimum conditions, we exploit the unpredictability of the system for the application of random bit generation.

In this introductory Chapter, the basics for the understanding of the Thesis are reviewed, introducing delay systems and emphasizing the role of photonic systems for the investigation of complex dynamics. The concept of consistency in nonlinear delay systems is explained together with the property of unpredictability resulting from the chaotic dynamics, and relate it to the application of random bit generation. In this way, the reader will be prepared for the following chapters and the results they contain. The mathematical methods to quantify consistency and unpredictability can be found in Chapter 2.

1.1 Delay systems

The presence of delay in dynamical processes in real life is undeniable [1]. Time delays are, in our reaction times, determined by the time our brain requires to process information and send an order to our muscles [2]. Examples abound, such as in traffic dynamics, where cars are followed by other cars and drivers have to adjust their speeds accordingly [3], or in heating systems where one needs to set a given water temperature [4], and even in more sophisticated structures like the airport networks where delays are propagating around the globe [5].

The appearance of a delay time in a simple dynamical system often results in a completely new phenomenology. It has been shown that delay induces instabilities that can alter the dynamical behavior by exhibiting oscillations or even chaos [1]. These delay-induced instabilities can be considered an inconvenience to be avoided in engineering applications. Nevertheless, delay is something of a double-edged sword. There are situations in which the delay plays a stabilizing role and can be used to non-invasively control unstable states [6, 7]. Such interesting aspects of delay systems stimulated the study of the induced phenomena in physical systems which benefited from the cross-fertilization between theory and experiments, and the possibility to use the gained knowledge in novel applications.

From a mathematical point of view, systems with discrete delay are described by delay differential equations of the form:

$$\dot{\mathbf{x}}(t) = F(\mathbf{x}(t), \mathbf{x}(t-\tau)) \qquad \mathbf{x}(t) \in \Re^N. \tag{1.1}$$

Where x is the state of the system given by its N degrees of freedom, F is any linear or nonlinear function, and $\tau>0$ is the delay time. The appearance of a delayed term in a differential equation leads to drastic changes in the analysis. This is due to fact that the solution is no longer uniquely defined by a single initial condition but, at any time t_0, the solution profile of the variables within the interval $[t_0\text{-}\tau,\ t_0]$ is needed to define the state of the system. This implies that the initial condition is the equivalent to a vector in phase space, and that the phase space becomes formally infinite dimensional, allowing the existence of attractors with high dimensions. Nevertheless, the dimensionality of the delay dynamics remains finite in practice.

1.2 Photonic delay systems

Despite the ubiquity of delay systems, a large contribution to the study of delay dynamics have been made through semiconductor laser systems. The versatility, compactness and robustness of their performance made semiconductor lasers ideal test-beds for the study of nonlinear dynamics, and in particular, good representatives for the study of delay systems. Since the invention of semiconductor lasers in 1962 [8, 9, 10], their use has been expanding to endless applications and technological advances, making the research in the field of photonics a continuing emerging area with a substantial economic impact. Semiconductor lasers are characterized by a strong sensitivity to delayed feedback or delayed coupling, meaning that, even when a tiny fraction of light reenters into the cavity of the laser, the emission properties are significantly perturbed [11, 12, 13, 14]. The feedback induced instabilities result in the emergence of complex dynamical scenarios, far from the stable steady emission expected from a laser. Such complex dynamics have been investigated extensively [15, 16, 17, 18]. Nevertheless, the original motivation for its study was to get rid of most of the delay-induced dynamics, since their presence implies the degradation of the performance in real-world applications like the CD/DVD players or in telecom modules. It was in the early 1990s that their advantageous attributes started to be recognized, mainly in the field of chaos applications [17, 19]. With the fast time scales of the chaotic oscillations over frequencies of gigahertz, the instabilities in semiconductor lasers turned out to be an important attribute for modern chaos communications [20] or chaos encryption [21, 22], but also as low-coherence sources for rainbow refractometry [23], remote position sensors, lidars [24], random bit generators [25] or information processing [26], among many others.

It is worth mentioning that complex dynamics is here understood as all nonlinear dynamical phenomena emerging from the delayed feedback [27, 28, 29, 30, 31]. Periodic oscillations [32, 33] and period-doubling [34, 35], quasi-periodicity [36], deterministic chaos [37, 38, 39, 40, 41, 42, 43, 44, 45, 46], multistability [38], bifurcation cascades [47, 48, 49], intermittency [50], and chaos synchronization [51, 52, 53] are some of the nonlinear behaviors observed in photonic delay systems.

1.2.1 Photonic delay systems in the drive-response scheme

Semiconductor lasers are not only sensitive to their own delayed feedback but the addition of an external driving signal to the laser also perturbs the emission properties. Photonic delay systems represent a good platform for the investigation of drive-response schemes. In such schemes, the drive system generates an output signal that is sent to the response system, which in this case is a system with delay (see Fig. 1.1 (a)). Then, the reactions of the response system to the drive are analyzed. The drive is usually a direct parametric modulation of the laser pump current, but more elaborated drives can be utilized. A delay system can also act as a drive when its output is injected into a response system (which can be a delay system or not), as illustrated in Fig. 1.1 (b). One could even think of a single laser with delay feedback

as self response system, where the output signal x(t) is the response to the drive x(t-τ) like in Fig. 1.1 (c). In a more elaborated setup, a single delay system with multiple feedback loops could serve as a drive and response system at the same time (see Fig. 1.1 (d))). While the use of an external driving signal restricts the origin of the drive to electrical scalar recorded waveforms, the possibility to use photonic delay systems also as drives (Fig. 1.1 (b), Fig. 1.1(c) and 1.1(d)) permits the utilization of complex continuous vector-state optical drives. Along this Thesis, different schemes of drive-response systems are used.

The drive-response configuration represents a prominent base for the investigation of a crucial property of nonlinear systems: consistency.

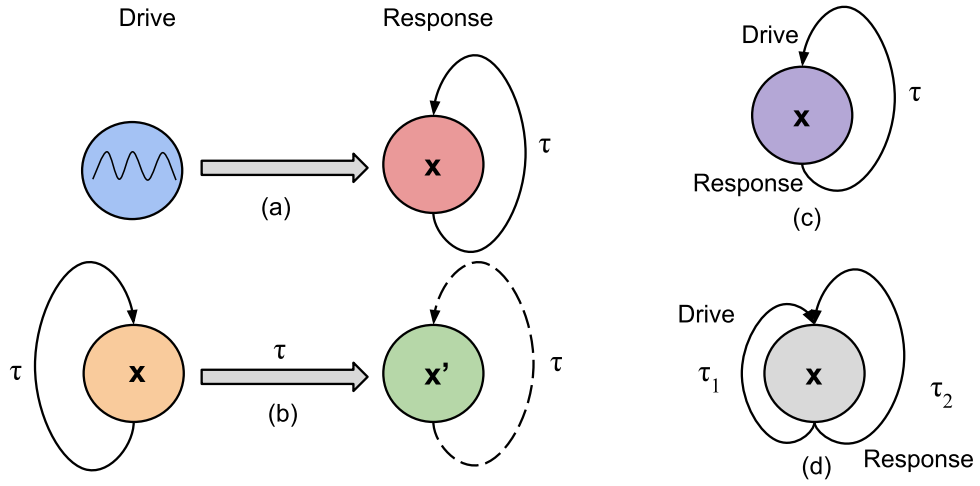

Figure 1.1: Illustration of four possible schemes employed for the investigation of drive-response systems. The delay system is used as response system. (a) Any arbitrary signal can be used as a drive. (b) The output of a delay system serves as the drive of a response system, which can be a delay system or not. (c) A single laser as self response system. (d) A delay system with two feedback loops.

1.3 About Consistency

In real life applications, it is an obvious requirement to have a reliable operation of a given system. This means assuring the same (or very similar) performance of the system when tested repeatedly. In nonlinear dynamical systems, we call this property consistency. Consistency is defined as the ability of a nonlinear system to respond in a similar manner to similar inputs [19]. This definition can be easily interpreted in terms of drive-response schemes, so that similar drives lead to similar responses, without imposing any restriction on the types of drive signals used. The nature of the drive signals can be optical or electrical, and their

origin can come from real recorded time traces of the system, from noise, from artificially generated waveforms with an Arbitrary Waveform Generator, or any other source. Consistency is, therefore, a non-trivial property of the response system that depends on the drive. For a certain input, a system might provide a consistent response, whereas the same system can exhibit inconsistent behavior for another drive. This is illustrated in Figure 1.2.

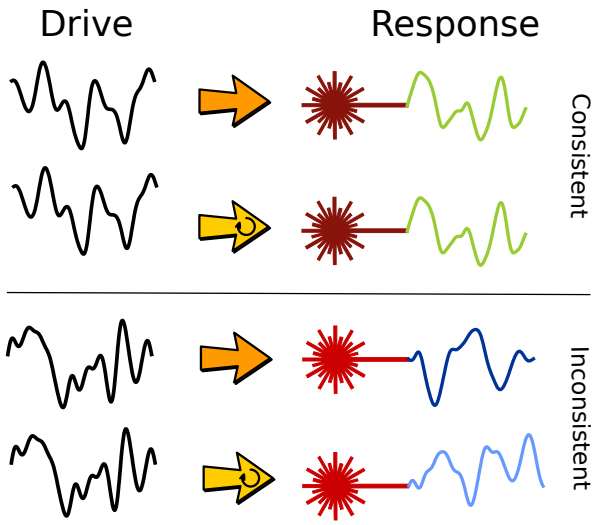

Figure 1.2: Illustration of the concept of consistency. The same system can exhibit consistent or inconsistent responses depending on the drive. When repetitions of the same drive lead to a similar response, there is a consistent behavior of the system. But if repetitions of a drive signal lead to significantly different responses, the system is inconsistent.

The boundaries between consistent and inconsistent behavior are not well defined, and the responses of a dynamical system can be classified into a certain degree of consistency. Responses that are structurally similar but not identical can still be considered consistent. But in a more restrictive scenario, we can distinguish *complete* consistency as the case in which the same input leads to the exact same output of the system. Consistency has also been referred to as reliability and often investigated under the terms of generalized synchronization or noise synchronization [54]. In Chapter 2, the concept of consistency with the notion of generalized synchronization is discussed.

1.3.1 Applications of consistency

There is a clear connection between consistency and the analysis of brain dynamics. The brain, although a complex system, exhibits various degrees of consistency in the neuronal functionality in response to repetitions of input signals and stimuli [55]. This phenomenon has commonly been referred under the term reliability. Consistency also partakes in the formation of spatio-temporal patterns in motor learning [56]. The investigation of the fun-

damental mechanisms behind the achievement of consistency can be useful to understand brain dynamics and the process of learning in the brain. Neuronal systems and photonic delay systems share some common phenomena that make the latter good candidates for such investigations. Both systems can exhibit zero-lag synchronization despite their delays in propagation, and the topology of the configuration is also crucial in both systems for the achievement of synchronization dynamics. The many similarities between the dynamical properties of neuronal networks and photonic delay systems have also led to the development of a bio-inspired information processing concept, the so called Reservoir Computing, whose performance strongly depends on the consistency properties."

In Reservoir Computing, a nonlinear delay system has been proposed and demonstrated successful for the performance of complex tasks such as speech recognition [26, 57]. The method uses the scheme of drive-response system, and a consistent (or reliable) response output with respect to a drive signal is required for the successful implementation of this machine-learning tasks. However, the uses of consistency surpass the processing of information.

Consistency is a concept that shows up in many other fields where the scheme drive-response is present. The success of many practical applications relies on the reproducibility of the dynamical behavior to guarantee the robustness of the system. In biology, the response of biomolecules to external inputs can be tested and used to identify severe changes in the system. In engineering, a consistent behavior is a basic requirement for the development of new materials when assessing their mechanical properties. It is also essential in cryptography for the generation of secure tokens, where the drive-response relation must be complex and at, the same time, reproducible [19].

So far, we have introduced the property of consistency in nonlinear systems. A semiconductor laser system with delay can display a complex yet reproducible behavior and, thus, predictable. Interestingly, and as explained in the next section, the same system can also act as a source of unpredictable dynamics, broadening the uses of photonic delay systems.

1.4 About Unpredictability

Among the different dynamics generated by photonic delay systems, deterministic chaos is one of the most prominent and investigated behaviors. Chaos is a phenomenon characterized by irregular oscillations in a nonlinear system with a strong dependence on initial conditions [58]. This means that any two trajectories that start close to each other will separate exponentially with time, Figure 1.3. Nevertheless, chaos is deterministic which means that, if the initial conditions are known with infinite precision, the irregular behavior can be reproduced. Knowing the initial conditions without error is an inherently unrealistic abstraction in continuous dynamical systems but, still, chaos should not be taken as a synonym for randomness or stochasticity.

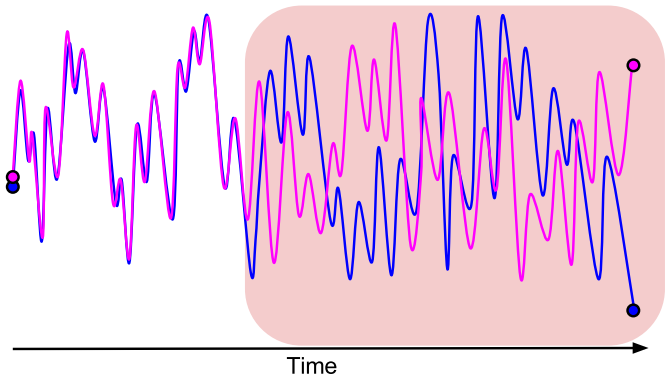

Figure 1.3: Sensitivity to initial conditions: two trajectories that begin close to each other separate exponentially with time.

In practice, the distinction between a random and a chaotic process from experimental data can be a hard task to achieve. Often, the methods rely on tracking the evolution of two nearby trajectories but the identification of close states in high dimensional systems demands big amounts of data and computations.

In photonic systems, semiconductor lasers with time delayed feedback produce fast dynamical instabilities that can lead to deterministic chaos. Semiconductor lasers with delayed feedback, as real chaotic systems, also exhibit a stochastic contribution in their dynamics. Noise additions from the spontaneous noise emission of the laser, and also from the experimental devices that form the setup, are unavoidable. The noise is amplified due to the inherent nonlinearity of the system giving rise to random-like dynamics. Therefore, it is the actual interplay of chaos and noise that makes these systems an outstanding implement for unpredictable behavior.

1.4.1 Applications of unpredictable dynamics

In a world in which digital technologies are established in our everyday lifes, the demands for security in network communications and data transmission have led to the development of new encryption protocols. The use of the chaotic dynamics of semiconductor lasers represents a good approach, given the possibility to operate at high speeds and their easy implementation in current optical communication channels.

One current application that benefits from the combination of chaotic dynamics with inherent noise is random bit generation [25]. The chaotic output of a semiconductor laser is sampled with a fast oscilloscope, converted into a stream of binary numbers and post-processed, resulting in random bits that can pass sophisticated tests of randomness. We elaborate on this application in Chapter 6, in which a practical implementation of a fast random bit generator based on a laser with polarization rotated feedback is demonstrated.

Another important application is chaotic secure communications based on chaos synchronization between two nonlinear systems [22, 59, 60]. Two independent chaotic laser systems

exhibit different autonomous dynamics due to the uncertainty in their initial conditions. However, the two systems can synchronize when coupled, that is, when a small portion of the chaotic output from one system is injected in to the other. This principle serves as the key for chaotic encryption and decryption of messages and secure exchange of a private key through a public channel [61, 62].

Other uses of chaotic lasers in optical sensing include the correlation or chaotic radar (CRADAR) based on chaotic pulse trains with high pulse repetition frequencies that allow for high precision range measurements [63, 64]. In the field of computing, optical logic gates have been implemented via the synchronization properties of two chaotic lasers [65]. These applications are only a few examples of the possibilities of chaotic photonic systems. New exciting developments of chaotic dynamics in semiconductor lasers are yet to come.

1.5 Overview of this Thesis

The work in this Thesis is devoted to the study of photonic delay systems as a source of a great variety of complex dynamics that can ensure reliable behavior as well as unpredictability. The property of consistency is investigated from a fundamental point of view with the characterization of the responses from different laser systems and driving sources. The unpredictability property is exploited in the cryptographic application of random bit generation.

- In Chapter 2, we present the methods and tools used to quantify consistency and unpredictability, and discuss the relation between consistency and generalized synchronization.
- In Chapter 3, we investigate the consistency properties of a semiconductor laser system to its own time-delayed signal. A scheme with two different feedback loops is utilized to store a copy of the dynamical features with high precision and inject it at a later time. The consistency is quantified in terms of correlations and, for the first time in experiments, with a measure proportional to the sub-Lyapunov exponent, the σ value.
- In Chapter 4, a laser with delayed feedback, operating in the regime of Low Frequency Fluctuations, is employed for the characterization of consistency to an external drive in the form of short pulses. The feasibility of induced intensity dropouts in the dynamics is analyzed with different pulse distributions. The inter- and intra-correlations are calculated to demonstrate the role of the drive pattern.
- Chapter 5 covers the use of an opto-electronic intensity oscillator to explore its consistent behavior when different external drives are applied. As a scalar system with multistability, new dynamical features emerge under the influence of a drive. Harmonic signals, pseudo-random pulses and time-traces originating from the system are used as modulation. The correlations indicate a significant level of consistency even in a global chaos regime.

- Chapter 6 focuses on the exploration of unpredictable dynamics from a laser system to the application of random bit generation. Optimum operating conditions are identified, and guidelines on the interplay between dynamics, acquisition process and postprocessing procedures are discussed to guarantee the randomness of the bits.
- The last Chapter of this Thesis includes a summary of the achievements, and an outlook and perspectives for future work.

CHAPTER 2

Concepts and tools

> It is a recurring experience of scientific progress that what was yesterday an object of study, of interest in its own right, becomes today something to be taken for granted, something understood and reliable, something known and familiar – a tool for further research and discovery.
>
> J. Robert Oppenheimer, Physicist

This Chapter covers the mathematical tools employed to quantify consistency and unpredictability throughout the Thesis. Regarding the concepts, a discussion on the equivalence between consistency and generalized synchronization, two closely related terms, is also included. To measure consistency, we introduce the sub-Lyapunov exponent, used in Chapter 3, and the inter- and intra-correlations, employed in Chapters 4 and 5. These two quantities provide different and valuable information about the responses of a driven system. In the last section, we review the well-established tools available to quantify unpredictability, like entropy or autocorrelation function, and we discuss other indicators of the randomness of a time series.

2.1 Consistency and Generalized Synchronization

Consistency is often put in context with generalized synchronization [66, 67, 68]. It should be noted that differences between the interpretations of consistency and generalized synchronization need to be taken into account, and the two terms cannot be utilized synonymously. Generalized synchronization in driven systems is understood as the existence of a functional relationship between the state of the driven system y with another dynamical system x that

acts as the arbitrary drive (Fig. 2.1 (a)).

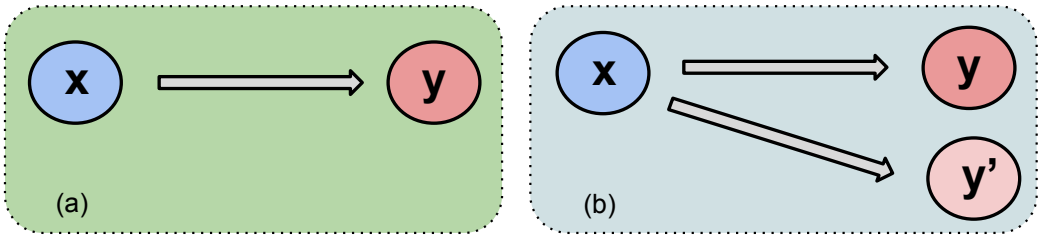

Figure 2.1: (a) Drive-response scheme for generalized synchronization. (b) Scheme for the extended generalized synchronization with a replica system y'.

Consistency and generalized synchronization already present a major dissimilarity in the point of view: generalized synchronization describes a property of the relationship between coupled systems while consistency is a property of the response system. The fact that the definition of consistency is based on the "similarity" of the responses makes it a difficult concept to be described and quantified mathematically. Whereas consistency implies a broad set of possible outcomes, ranging from inconsistent to complete consistent responses, generalized synchronization only contemplates a subset of consistency: complete consistency. In the drive-response scheme like the one depicted in 2.1 (a), complete consistency and generalized synchronization are indeed equivalent. If the drive and response systems are in a state of generalized synchronization, in which stability is implied, the responses to the drive will have complete consistency and viceversa. Nevertheless, if the responses are not completely consistent, but have a high degree of consistency, the system will not exhibit generalized synchronization. This could be the case, for instance, when the responses are not identical but are still narrowly bounded.

If we extend the concept of generalized synchronization, as in the Abarbanel test [67], we can denote as extended generalized synchronization the situation in which a copy of the system y' subject to an arbitrary drive x receives the same input and, thus, exhibits complete synchronization with the original y, as depicted in Fig. 2.1 (b). With this scheme, the replica system y' serves to test the repetition of the input x. Again, the three properties (generalized synchronization between x and y, complete synchronization between y and y', and complete consistency of y) would be equivalent. However, as soon as we leave the unidirectional scheme $x \Rightarrow y$ to other arbitrary schemes, the equivalence between properties becomes non-trivial. For example, a mutually coupled scheme $x \Leftrightarrow y$ can already alter the possible outcomes. The functional relationship between the states of drive and response may be undefined, but x and y may still be consistent when the replicas are attached, and viceversa.

To summarize, the extended generalized synchronization is equivalent to complete consistency as a local property of a driven system, no matter the origin of the drive. When the scheme is not a unidirectional drive-response setup, the equivalence between the two concepts

does not apply anymore, and the presence of a generalized synchronization manifold does not imply consistency.

2.2 Tools to measure consistency

There are different ways to measure consistency that take into account the type of drive. Here, we introduce two different tools to quantify the degree of consistency. One is based on the calculation of the sub-Lyapunov exponent, and the other is based on the calculation of correlations. The sub-Lyapunov exponent characterizes the response of a driven system in terms of stability and requires the access to the error between the two response signals. The sensitiveness to mismatches between the two responses makes this method more oriented to non-scalar high optical bandwidth drives that can be repeated with high accuracy. The calculation of the correlation coefficient between responses is a practical method that can directly quantify the level of consistency. Their fast computation times and the possibility to use them to identify patterns in the responses makes it more suited for external scalar drive signals that are reinjected multiple times.

2.2.1 The sub-Lyapunov exponent

In dynamical systems, and particularly in chaotic systems, the sensitivity to the initial conditions is often described by the Lyapunov exponent λ, which measures the mean rate of the separation between two nearby trajectories. For a given dynamical system with a state vector $\mathbf{x}(t)$ evolving like in Eq. 2.1:

$$\dot{\mathbf{x}}(t) = f(\mathbf{x}(t)) \qquad \mathbf{x}(t) \in \Re^d \tag{2.1}$$

we can linearize the temporal evolution of a small separation (or perturbation) $\delta\mathbf{x}(t)$:

$$\dot{\delta\mathbf{x}}(t) = Df(\mathbf{x}(t)) \cdot \delta\mathbf{x}(t) \tag{2.2}$$

so that for a given trajectory $\mathbf{x}(t)$, the maximal Lyapunov exponent is defined by:

$$\lambda = \lim_{t\to\infty} \frac{1}{t} \ln\{\frac{||\delta\mathbf{x}(t)||}{||\delta\mathbf{x}(t_0)||}\}. \tag{2.3}$$

There is a whole spectrum of Lyapunov exponents, which in the case of an autonomous system, equals the dimensionality of the phase space (or in other words, same number of Lyapunov exponents as system variables). In delay systems though, the spectrum of Lyapunov exponents is formally infinite. However, we focus on the maximum Lyapunov exponent,

which gives a notion of the predictability of the system and connects the local stability with the global dynamics. A positive maximal Lyapunov exponent indicates chaotic dynamics. A negative maximal Lyapunov exponent is associated with a steady state dynamics, and a λ=0 could indicate a periodic or quasi periodic orbit in phase space.

The Lyapunov exponents are a property of the system, which allow for other derived measures like the Kolmogorov-Sinai entropy or the Kaplan-Yorke dimension, related to the complexity and dimensionality of the system.

Pecora and Carroll [51] introduced the concept of the sub-Lyapunov exponent as a property of a subsystem belonging to a chaotic system. To investigate the synchronization properties of chaotic coupled systems, they considered an autonomous system with phase space vector $\mathbf{u}$ and divided it into two subsystems $\mathbf{v}$, $\mathbf{w}$. The subsystems obey the equations of motion:

$$\begin{aligned} \dot{\mathbf{v}}(t) &= g(\mathbf{v}(t), \mathbf{w}(t)) \\ \dot{\mathbf{w}}(t) &= h(\mathbf{v}(t), \mathbf{w}(t)) \end{aligned} \tag{2.4}$$

They observed that, under certain conditions, a copy of $\mathbf{w}$, $\mathbf{w}'$, can be made to synchronize with the original $\mathbf{w}$ if both receive the same signal. To prove it, they followed a similar approach, linearizing with respect to $\mathbf{w}$ and writing the equations for a small perturbation of the synchronized state $\xi(t)$:

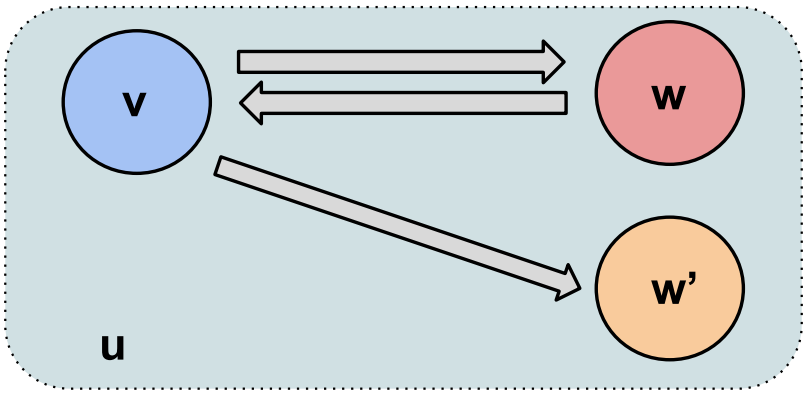

Figure 2.2: An autonomous system $\mathbf{u}$ is divided into two subsystems $\mathbf{u} = \mathbf{u}, \mathbf{w}$ and a copy $\mathbf{w}'$ is created to test the synchronization properties.

$$\dot{\xi}(t) = D_w h(\mathbf{v}(t), \mathbf{w}(t)) \cdot \xi(t). \tag{2.5}$$

From this equation, the maximal Lyapunov exponent of the subsystem can be obtained, also known as sub-Lyapunov exponent λ_0:

$$\lambda_0 = \lim_{t\to\infty} \frac{1}{t} \ln\{\frac{||\xi(t)||}{||\xi(t_0)||}\}. \tag{2.6}$$

When λ_0 is negative, there is complete synchronization between $\mathbf{w}$ and $\mathbf{w}'$. There are as many sub-Lyapunov exponents as dimensions of the subsystem $\mathbf{w}$. One can identify this system as a drive-response scheme, in which an autonomous subsystem acts as the drive of another subsystem, the driven system. For the latter, the maximal sub-Lyapunov exponent can be defined, and measures the convergence of the response states to a function of the drive.

In this Thesis, all the schemes investigated are delay systems, with a temporal evolution given by Equation 1.1. The sub-Lyapunov exponent of delay laser systems quantifies the consistency with respect to small perturbations in the response of a semiconductor laser subject to its own time delayed feedback. The sign of the sub-Lyapunov exponent determines whether the laser behaves in the same way when the external input is repeatedly applied, so that a negative λ_0 would indicate an exponential decay rate of the small perturbation to the consistent state.

The sub-Lyapunov exponent has been linked to the concept of strong and weak chaos. These two terms refer to two different types of chaos identified in networks of time-continuous systems with time-delayed couplings. Thus, delay instabilities can be categorized depending on the scaling properties of the maximal Lyapunov exponent [69, 70]. In the large delay times, the maximal Lyapunov exponent converges to a nonzero value in the presence of strong chaos but, in the case of weak chaos, the maximal Lyapunov exponent scales with the inverse delay time. From the point of view of delay systems in the drive-response scheme, the sub-Lyapunov exponent represents a direct measurement of the type of chaos. A positive syb-Lyapunov exponent indicates strong chaos dynamics, while a negative sub-Lyapunov exponent implies weak chaos. For synchronization purposes, it has been shown that only networks with weak chaos can synchronize to a chaotic signal. The sub-Lyapunov exponent is also defined outside delay coupled networks, which then emerge as a special case of drive-response systems if the delay couplings are considered as drives for the individual nodes. Using the extended notion of the sub-Lyapunov exponent, an analogue to weak chaos can be identified with the complete consistent response, and strong chaos with a non-completely consistent response. Jüngling [71] developed an algorithm to extract the value of the sub-Lyapunov exponent from stationary chaotic time series of a delay system. In Chapter 3, a method to measure a quantity proportional to the sub-Lyapunov exponent, σ, is explained in detail.

2.2.2 Inter- and intra-correlations

Complementary to the widely used correlation coefficients, in the cases where an external modulation is repeatedly injected to the system, we use the so-called inter-correlation and

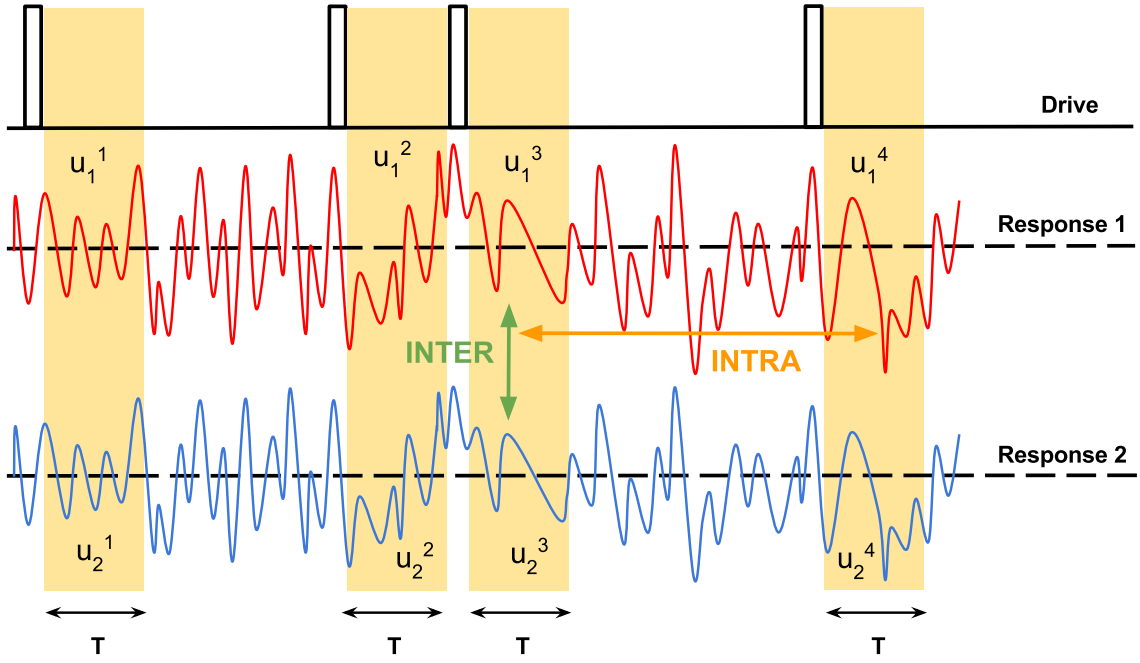

Figure 2.3: Illustration of the concepts of inter- and intra-correlations. Two trajectories are depicted in response to a pulsed drive. 4 responses $u_i^j(t)$ of duration T are compared within the same time trace (intra-correlation) and among the two repetitions (inter-correlation).

intra-correlation measures. The input drive can be an harmonic function, a random distribution of pulses or even a noisy signal, with or without periodicity. The intra-correlation compares the response trajectories of the system along the same input drive, whereas the inter-correlation compares the responses across multiple repetitions of the same input drive. These two types of correlations, developed by Jordi García-Ojalvo and Javier Buldú, are illustrated in Figure 2.3.

Let the drive be a sequence of N pulses or an harmonic function of N periods, and M the number of time traces corresponding to the repetitions of the modulation sequence. We denote the response of the system to a given pulse or period as $u_i^j(t)$ with $t \in [0, T]$. Here, i indicates the repetition of the sequence, so that $i \in [1, M]$, and $j \in [1, N]$ defines the index of the pulse or period along the sequence, so that NT is equivalent to the total duration of the sequence. The duration of the responses T coincides with the period of the modulation or the minimum spacing between pulses.

To compute the correlations, we altered the original expression of the pairwise-based Pearson coefficient. For two given responses, u_i^j and u_k^l, the Pearson coefficient would be

calculated as:

$$C_{u_i^j,u_k^l} = \frac{\langle (u_i^j - \mu_{u_i^j})(u_k^l - \mu_{u_k^l}) \rangle}{\sigma_{u_i^j}\sigma_{u_k^l}} \tag{2.7}$$

The new expression uses a global mean μ_{global} and variance σ^2_{global} instead of product of individual standard deviations:

$$C_{u_i^j,u_k^l} = \frac{\langle (u_i^j - \mu_{global})(u_k^l - \mu_{global}) \rangle}{\sigma^2_{global}}, \tag{2.8}$$

where μ_{global} is the mean of the ensemble of all the responses. In this global normalization, all the responses are concatenated into a time series, and then normalized as a whole. In the case of a pulsed drive, it excludes the pulses. This causes a centering around zero that highlights the small differences in the amplitudes of the responses. This new method to compute correlations is capable to highlight subtle changes between responses that, with the locally normalized coefficient, would have remained hidden. An example of this could be two responses characterized by a positive growth of the power intensity but with different slopes. The new global centering would distinguish the two types of responses with a lower correlation value than the Pearson coefficient. Whether for the calculation of μ_{global} and σ^2_{global} one uses the time traces excluding the pulses, or just the portions of time traces corresponding to the windows used for the correlation, is a free choice. In the following, the results shown correspond to the second case. The final correlation would then be given by the average of all the pairwise calculated values.

We can now define the intra-correlation as the correlation for responses along the same sequence:

$$C_{intra} = \frac{1}{MN(N-1)} \sum_{k=1}^{M} \sum_{i=k}^{M} \sum_{l=1}^{N} \sum_{\substack{j=1 \\ j\neq l}}^{N} \frac{\langle (u_i^j - \mu_{global})(u_k^l - \mu_{global}) \rangle}{\sigma^2_{global}} \tag{2.9}$$

This formula calculates, for every repetition i of the drive, the correlation of each response window with the rest of the responses, excluding the self ones.

The inter-correlation is defined as the correlation for the same response window across different repetitions of the drive:

$$C_{inter} = \frac{1}{MN(M-1)} \sum_{k=1}^{M} \sum_{\substack{i=1 \\ i\neq k}}^{M} \sum_{l=1}^{N} \sum_{j=l}^{N} \frac{\langle (u_i^j - \mu_{global})(u_k^l - \mu_{global}) \rangle}{\sigma^2_{global}}. \tag{2.10}$$

Equation 2.10 calculates the correlation of the same response window l across the multiple repetitions k of the drive, excluding the self ones.

There is another way to compute these correlations with less computational demand based on an ensemble of responses, where the term ensemble refers to the set of all responses. For

that, the ensemble needs to be centered and globally normalized. The normalization should be performed again as if all the responses were concatenated to a new time series. The criteria can be expressed as:

$$\frac{1}{MN}\sum_{i,j}\frac{1}{T}\int_0^T dt\ u_i^j(t) = 0 \tag{2.11}$$

$$\frac{1}{MN}\sum_{i,j}\frac{1}{T}\int_0^T dt(u_i^j(t))^2 = 1. \tag{2.12}$$

A well-behaved intra-correlation based on the globally normalized ensemble compares all the individual responses, similar to the pairwise correlation coefficient, and averages over the repetitions.

$$C_{intra} = \frac{1}{(N^2-N)M^2T}\sum_{j\neq l}\sum_{i,k}\int_0^T dt u_i^j(t)u_k^l(t) \tag{2.13}$$

This formula correlates all the individual responses without excluding any particular combination except the self one. Limiting the intra-correlation to calculations within the same sequence would only affect the normalization factor. Analogously to the intra correlation, the globally normalized inter-correlation can be written as:

$$C_{inter} = \frac{1}{(M^2-M)NT}\sum_{j\neq l}\sum_{i,k}\int_0^T dt u_i^j(t)u_k^l(t). \tag{2.14}$$

However, another helpful expression can be derived for the calculation of the inter-correlation through the distance of the individual responses to their mean, which gives an idea of the ensemble spread. We can write the ensemble mean $\tilde{u}^j$ that depends on the event j:

$$\tilde{u}^j = \frac{1}{M}\sum_i u_i^j(t). \tag{2.15}$$

And we can calculate the distance of the individual responses to their ensemble mean as:

$$D_j^2(t) = \frac{1}{M}\sum_i (u_i^j(t) - \tilde{u}^j(t))^2. \tag{2.16}$$

It can be shown that the distance of a response to the ensemble mean is connected to the inter-correlation like:

$$C_{inter} = 1 - \frac{1}{1-1/M}\frac{1}{NT}\sum_j \int_0^T dt D_j^2(t). \tag{2.17}$$

where the normalization factors contemplate the projection of all the responses to a certain event onto each other excluding the self-projection. This is a useful expression that permits to split the correlation into meaningful contributions and distinguish for an event-dependent correlation.

The inter- and intra-correlations are very intuitive measures for consistency. A high correlation value would indicate a consistent response of the system, whereas a low correlation value would suggest an inconsistent response. The inter-correlation is an indicator of the reproducibility of the amplitude pattern for a given response. A correlation of 1 would correspond to a complete consistent response, meaning that the responses would overlap into a narrow line. With a correlation of 0, the ensemble of responses would display an unstructured distribution.

The intra-correlation compares responses to different events. This might be of interest to identify whether consistency depends on the occurrence of a certain event or, on the contrary, the system responds consistently to any sort of perturbation. The first case should translate into a high inter-correlation and lower intra-correlation, while the latter should display similar inter- and intra-correlations. This method also allows for a whole gradient of consistency, and can provide insights into the memory capabilities of the system when the repetitions are compared.

Inter- and intra-correlations also unveil important information on the statistical properties of the nonlinear system. Using a pseudorandom pulsed sequence as example of modulation, every occurrence of a pulse is acting as a trigger for the evaluation of the responses. If one interprets the inter-correlations as an ensemble average of the responses, provided that it uses repetitions from the same trigger, and the intra-correlations are considered a time average between different responses from different trigger points, the inequality between the two quantities would reveal that the system is not ergodic in this sense [72].

Focusing on the intra-responses, their dissimilarity can illustrate the time scales at which the memory effects remain. If the separation between the pulses were long enough, the trajectories would have enough time to reach the attractor after the perturbations, and therefore, we would not expect much difference between the inter- and intra-correlations. But in cases in which the influence of the previous pulses is visible, the time scale of the memory is larger than the intervals between the perturbations, preventing the trajectories to reach the stable attractor. Hence, under such circumstances, the inter-correlation values are higher than the intra-correlations.

2.2.3 Review of the consistency measures

Consistency is a property that lacks a rigorous definition so far and, consequently, of a mathematical framework with clear tools to quantify it. All the measured quantities rely on the

definition of consistency based on the similarity between responses, but no clear boundaries between inconsistent, consistent and complete consistent response have been determined. Depending on the drive-response system, different measures are suited to estimate the degree of consistency. Calculation of correlations in their different forms (Pearson coefficient, distance to a response, autocorrelations or distinguishing inter- and intra-correlations), have been employed to indicate the similarity of the responses. Their use is motivated by the ability to extract these quantities from experimental recorded data, specifically, from time traces of the dynamics.

Their interpretation is also very straightforward. The consistency correlation, understood as the correlation between responses (either inter or intra) to a repeated drive, is a meaningful measure that allows for a whole range of consistency, scaled from zero to one. A Pearson coefficient close to one also indicates that two responses are almost identical, but does not take into account differences in the offset of the responses. In a single system with delayed feedback, in which the delayed signal acts as an external drive, the autocorrelation function can be interpreted as a consistency measure too. The height of the delay echoes imply a high similarity in the trajectories, and thus, a consistent response to the self-delayed input.

All these measures can be good indicators of the consistency properties, although there are situations in which they might fail. For instance, experimental issues, like a poor signal-to-noise ratio, can easily induce inaccurate correlation values. In the case of a behavior, which in an ideal system would be completely consistent, the presence of mechanisms that could temporally alter the synchronization of the responses, such as bubbling, could lead to low correlation values, which would then be interpreted as not complete consistency or even inconsistency.

The sub-Lyapunov exponent is the quantity at the core of complete consistency, characteristic for the drive-response schemes. It affects the consistency properties of the response system and, in the case of delayed feedback systems, connects them directly with strong and weak chaos. In other words, the sub-Lyapunov exponent describes the conditional stability of the response of a dynamical system with respect to a certain drive. When the drive is a delayed feedback signal, a negative λ_0 indicates the presence of weak chaos. Under such circumstances, the response of the driven system is stable and can be consistent. With a positive λ_0, we operate in a regime of strong chaos and the response of the unit is not completely consistent. Yet it is difficult to extract the sub-Lyapunov exponent from experimental time traces.

Testing the consistency properties out of the complete consistency case becomes more intricate. The distinction between a high degree of consistency and inconsistency is not possible from the sub-Lyapunov exponent. Consequently, we recommend, when possible, a combination of both methods to characterize the consistency properties of the laser system. With the extraction of the sub-Lyapunov exponent and the correlation measures a good description of the consistency in a dynamical system can be achieved. Future methods to extract the sub-Lyapunov exponent, as well as the development of new tools to quantify consistency, will improve significantly the characterization of nonlinear systems.

2.3 Tools to measure unpredictability

Unpredictability is commonly measured by entropy rate [73]. In chaotic systems, unpredictability arises from the strong dependence on the initial conditions, so that small perturbations grow exponentially with time, limiting the abitility to predict future states. This sensitivity of the system to initial conditions can be quantified by the Kolmogorov-Sinai entropy, which is bounded by the sum of all positive Lyapunov exponents.

$$h_{KS} \leq \sum_{\lambda_i > 0} \lambda_i \tag{2.18}$$

Given that any microscopic noise in the chaotic system amplifies the divergence of two nearby trajectories in phase space, chaotic systems can generate random information [74, 75]. In the context of information theory, Shannon's formula for the entropy rate characterizes how quickly the system generates unpredictable information [76]:

$$H(t) = -\sum_{i=0}^{1} P_i(t) \log_2 P_i(t) \tag{2.19}$$

where $P_i(t)$ is the probability of occurrence of bit i (0,1) at the time t. As time evolves, the Shannon entropy increases, indicating a growth of uncertainty due to the spread of trajectories, and relates to the Kolmogorov-Sinai entropy. From experimental data, one can digitize the signal on one bit, so the chaotic dynamics can ideally generate up to one bit of entropy at a rate determined by the Lyapunov exponent. The time required for the system to reach an entropy value equal (or very close) to 1 is known as the memory time of the system.

By computing these quantities, one can estimate the rate at which random bits can be generated. Entropy calculations have also been used to explore the deterministic and stochastic aspects of a laser system used for random bit generation [74, 75]. Nevertheless, there are other measures that give an account of the unpredictability in the dynamics.

The autocorrelation function has been used to estimate the predictability: if future values of a time series depend on current and past values, the time series is predictable, and the dependence will show up in the autocorrelation function. The autocorrelation between times t and s for a process x is defined as:

$$AC(s) = \frac{< [x(t) - < x(t) >][x(t-s) - < x(t) >] >}{< [x(t) - < x(t) >]^2 >} \tag{2.20}$$

The autocorrelation function of the output of a semiconductor laser subject to delay feedback will present delay signatures at lags of the delay time τ. The height of the delay echoes serves as an indicator of the existence of repeating patterns in the dynamics, so a complete suppression of the correlation peak is desirable. This property can also be formulated as the

preference to operate in strong chaos conditions. The memory time effects of the system are also contained in the decay of the zeroth autocorrelation peak, providing insights into the independence of successive data points [77]. In addition to the autocorrelation function, the mutual information can be used to measure the uncertainty in the dynamics.

The unpredictability property of chaotic laser systems is mostly used in cryptographic applications, where the output of the laser needs to be chaotic, and to satisfy some noise-like features. The observation of some properties, although it cannot quantify the unpredictability, is key to guarantee a random behavior. The probability distribution functions of time series provide information about the appropriateness of the dynamics for unpredictability. Symmetrical distributions that resemble a Gaussian distribution are more favorable, and considered a good starting point for most chaotic applications. In terms of frequency components, the spectrum of an unpredictable time series should be broad, and have a flat power spectral density, similar to the white noise spectrum [77].

Other methods to estimate the unpredictability include the already mentioned calculation of the maximal Lyapunov exponent, the Kaplan-Yorke dimension or the phase space reconstruction of an attractor using data [19, 74, 75, 78].

CHAPTER 3

Consistency of a semiconductor laser to its own time delayed feedback

"The range of nonlinear dynamics is often largely underestimated."

Thomas Jüngling, Physicist.

3.1 Introduction

Consistency in dynamical systems has proven to be a powerful concept due to the ubiquity of drive-response schemes in nature and technology. The ability to respond in a similar way to similar inputs, starting each time from different initial conditions, is a necessary condition for the reliable operation of the systems. Cognitive tasks in neuron dynamics [79] or bio-inspired information processing [26, 57, 80, 81, 82] strongly depend on a consistent behavior. The first experimental work on consistency was introduced in 2004 by Uchida et al.[83]. In their experiment, a laser system is driven repeatedly by the same drive signal in order to describe the reproducibility of the responses. Recent numerical and experimental advances on consistency [84, 85, 86] also comprise the characterization of generalized synchronization properties of laser systems (see Chapter 1) driven by common light sources with fluctuating phase and or amplitude [87, 88, 89, 90, 91].

In this Chapter, we focus on two aspects of consistency that are critical for a controllable application. The first is the development of an experimental scheme providing a high quality repeated drive for fast experimental systems. To extend the investigations on consistency beyond the use of electrical drives, we need to design an experiment that allows to store non-scalar drives, such as optical signals, and inject them again while preserving the high optical and dynamical bandwidths. To achieve this, we employ a configuration of a photonic delay system with multiple feedback loops.

The second is the application and extension of time series analysis methods in order to reveal insights into the mechanisms underlying the consistency, like the extraction of the sub-Lyapunov exponent. Although the sub-Lyapunov exponent is at the core of the consistency property, up to now, it has not been possible to determine it experimentally. Small mismatches between response systems are sufficient to impede from its determination. There are only indirect indications for the transitions between consistent and inconsistent responses like spectral or intensity autocorrelation signatures of the laser dynamics in case of delayed feedback [92] or delay-coupled lasers [93]. However, the information contained in the delay echoes of the autocorrelation function can lead to misinterpretations. A high delay echo implies a similar repetition of the trajectory after a delay time, and can be seen as a consistent response of the system. But the Ikeda system [37] is the counterexample. This delay system has a constant sub-Lyapunov exponent for all the regimes investigated, although the shape of the autocorrelation changes with the parameters [94].

To explore the consistency properties, we employ a semiconductor laser subject to a drive originating from time-delayed optical feedback. It is well-known that delayed optical feedback induces high dimensional chaotic dynamics in semiconductor lasers [30]. Here, we use this mechanism as an ideal generator for complex optical drive signals. Therefore, we adapted the idea of a repeated drive [83] to the case of coherent and high bandwidth optical drive signals. Our scheme is based on two switchable feedback loops with significantly different lengths. This setup allows to store the optical drive in the long fiber loop while the short loop is active, and to replay it while the short loop is blocked. As a novelty, the replay offers all the features of the signal with high accuracy and without practical limitations with respect to optical and dynamical bandwidth. Even the optical phase dynamics is maintained, as long as the self-phase modulation does not become relevant. Moreover, in comparison to an equivalent generalized synchronization scheme using a replica system, we minimize mismatches by construction because the same laser is driven by the repeated signals. The combination of the small mismatches with the high quality of the replay allows for a direct quantification of the consistency properties experimentally with a measure proportional to the sub-Lyapunov exponent.

The results presented in this Chapter have been published as N. Oliver, T. Jüngling and Ingo Fischer, *Consistency Properties of a Semiconductor Chaotic Laser Driven by Optical Feedback*, Phys. Rev. Lett., vol. 114, 123905, March 2015. The experiments were performed by N. Oliver with the help of T. Jüngling. The analytical investigations and numerical simulations of sections 3.3.2 and 3.4 were carried out by T. Jüngling.

3.2 Experimental implementation

Figure 6.2 shows the simplified experimental scheme. The laser diode is an Eblana Discrete Mode Laser lasing at 1.54μm with a threshold current of the solitary laser of $I_{th} = 11.8$mA. The laser light is split to simultaneously enter two optical fiber loops, a short one with a

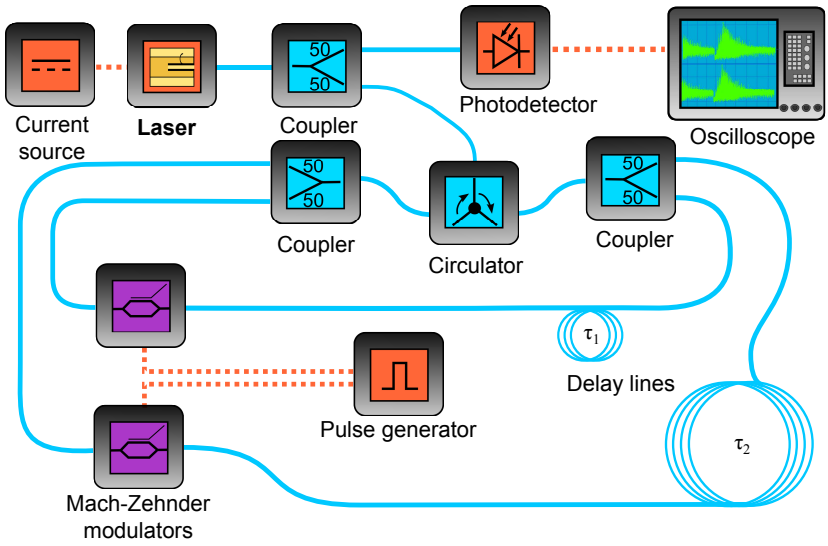

Figure 3.1: Experimental consistency setup. Figure from [86].

roundtrip time of $\tau_1 = 111$ns, and a much longer one with $\tau_2 = 21\mu$s. At the end of each fiber loop, the light passes through a Mach-Zehnder modulator. These electro-optical modulators are controlled by a pulse generator with a 50% duty cycle, such that when one path is closed, the other one is blocked. The period of the modulation is set to 50μs, and the switching time of the pulses is < 200ps. During the first 25μs, the laser receives feedback from the short delay loop, giving rise to the characteristic chaotic delay dynamics. When the short path is open and the long delay loop is active, the laser receives a replay of the optical field it already received a time $\tau_2 - \tau_1$ before.

We carefully designed and adjusted the system to obtain an exact repetition of the previous optical field, although the initial conditions of the laser are not the same. Temperature and pump current of the laser are controlled with an accuracy of ± 0.01K and ± 0.01mA, respectively. To obtain data of sufficiently high quality for the presented analysis, a strict control over the feedback parameters of the experiment is required. Therefore, other optical components, like polarization controllers and attenuators (not shown in the simplified scheme of Fig. 6.2), are set in the experiment to adjust and control the three following degrees of freedom:

- The first is related to the polarization state of the light. The short loop and the long loop must have the polarization state adjusted relative to each other as well as with respect to the laser output. Three polarization controllers placed along the experiment help in that task. The first one is settled right after the circulator to adjust the polarization of the light from the laser. The second and the third polarization controller are placed in the long delay loop, and in the common feedback loop entering back into the circulator, controlling the polarization of the feedback loops. By tuning the three polarization

controllers subsequently, a perfect match between the polarization state of the light from the feedback loops and the laser output is achieved.

- The second degree of freedom is related to the remaining transparency of the blocked loop. When a loop is active, the feedback light from the other loop needs to be suppressed. In order to achieve this, we added an external modulation to the laser, and monitored the spectrum of the intensity as detected by a photo diode with a realtime spectrum analyzer. We tuned the operating point of the Mach-Zehnder modulators in a way that the frequency signature of the modulation was imperceptible. With this procedure, a suppression of more than 25dB of optical power in the blocked loop can be achieved.

- Finally, short loop and long loop have to be equally transparent when they are active. Therefore, an attenuator in the short loop is used to guarantee the same level of transparency among the two loops with a precision of ± 0.01dB.

To facilitate the identification of the short loop and the long loop in the recorded time traces, we add a delay of $10ns$ between the switching process of the modulators. With this delay, every cycle of short-long loop dynamics contains $10ns$ in which both loops are blocked at the same time. The laser output is detected with a photodiode of 12.5GHz bandwidth and a digital oscilloscope with 16GHz analog bandwidth. After removing the transient intervals originating from the switching process, we compare the dynamics induced by the short feedback loop with the corresponding dynamics induced by the replay from the long loop to test consistency of the laser's responses. An illustration of the operation principle of the experiment is shown in Fig. 3.2.

3.2.1 Dynamical performance

The dynamical performance of the experiment can be seen in the spatio-temporal representations [95]. In such plots, the output power of the laser is color-coded, the horizontal axis represents the time up to the roundtrip time τ_1, and the vertical axis displays the 185 repetitions of τ_1 within each cycle. The spatio-temporal plots of the laser intensity output for the short loop cycle and for the long loop cycle are plotted in Fig.3.3(a) and (b) respectively.

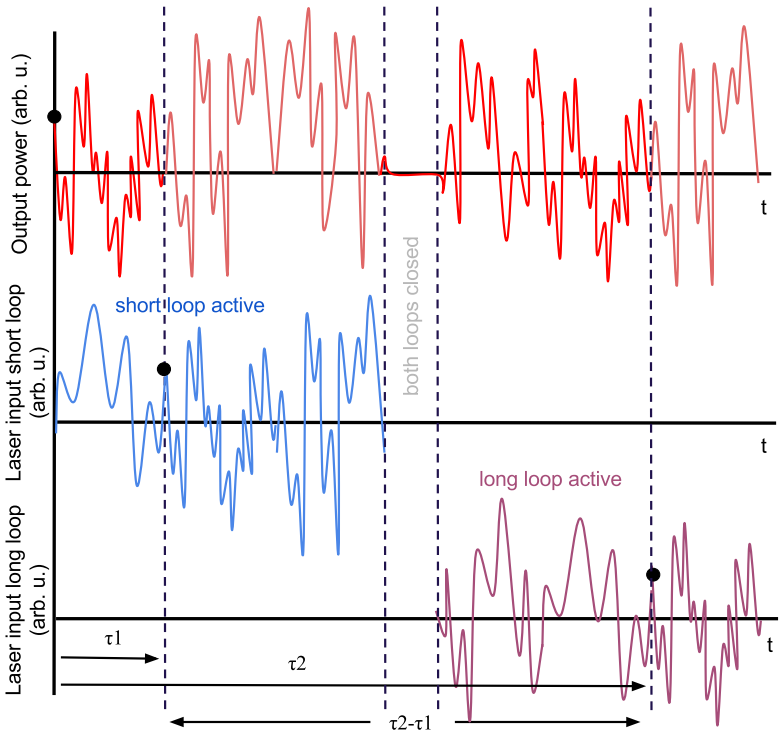

Figure 3.2: Schematic illustration of the operation of the setup. The first panel depicts the output of the laser. The second panel shows the operation of the short loop, which is active for $25\mu s$ (blue) and during that time, the laser evolves to its typical delay chaotic dynamics (red), while the long loop is blocked, serving as optical memory. During $10ns$, both loops are closed. When the long loop is connected (purple), the laser receives a copy of the optical field it received a time $\tau_2 - \tau_1$ before. The output of the laser from the short loop and the long loop with the corrected time deskew (light red) are then compared to test the consistency.

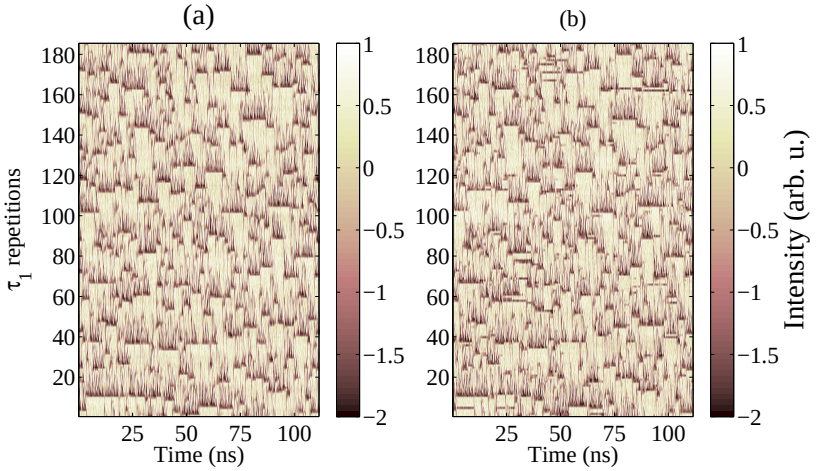

Figure 3.3: Space-time plots of the laser output acquired at I = $1.0I_{th}$ for (a) short loop cycle, (b) long loop cycle.

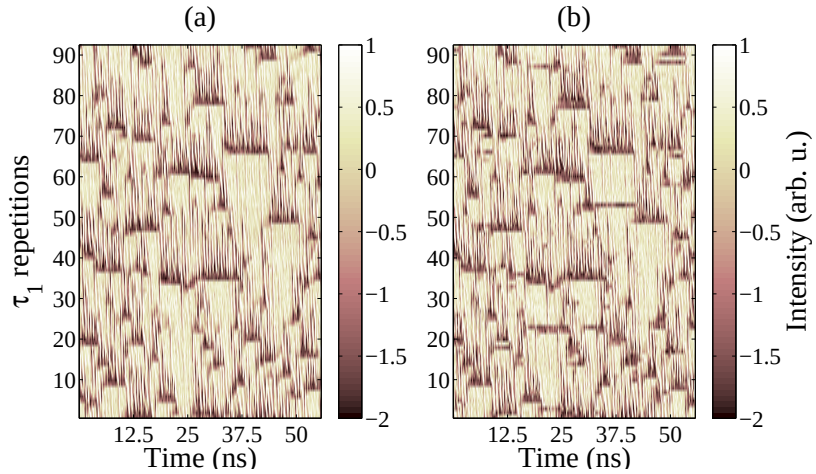

Figure 3.4: Zoom of the space-time plots of the laser output acquired at I = $1.0I_{th}$ for (a) short loop cycle, (b) long loop cycle. Figure from [86].

Fig.3.3(a) and (b) shows the spatio-temporal plots of the laser intensity output for the short and long loop respectively, acquired at I=$1.0I_{th}$. The dynamics is governed by chaotic intensity fluctuations including irregular power dropouts, characteristic of the chaotic feedback regime of Low Frequency Fluctuations (LFFs) [96, 97]. The dynamics in the LFFs regime exhibits a slow increase of the intensity, without reaching a stable level. They also present strong oscillations in the subnanosecond-scales until a dropout occurs. These spontaneous dropouts, represented in dark color, are present after some repetitions of the delay time. The dynamics induced by the short and long feedback loop exhibit the same patterns, illustrating the high accuracy of the replay and the consistency properties for the given conditions. A better visualization of the correspondence between short and long loop can be obtained from a zoom of the space time plots (Fig.3.4). The major differences, displayed as dark horizontal lines in Fig. 3.4(b), correspond to additional noise-induced dropouts occurring during the replay. Given that the short loop acts as the common drive, these dropouts are not maintained after one delay time τ_1, meaning that the system in the long loop cycle catches up to the original patterns and restores consistency. One should not misinterpret these features as impurities or noise effects; they are dynamical phenomena like intermittency or bubbling, which hamper the achievement of a perfect match between the two loops. Although Fig. 3.4 illustrates the good correspondence between the two responses, this is not a general characteristic. It is rather related to the particular dynamical regime which corresponds to a high level of consistency.

In contrast, Fig. 3.5 shows spatio-temporal plots of the laser output for the short (a) and long loop (b) acquired for a different pump current ($I = 1.27I_{th}$), by which we vary the dynamical properties. The laser dynamics are characterized by fast chaotic fluctuations, which makes the identification of the consistency properties hard on this entire scale. However, we can observe that Fig. 3.5 (a) and (b) are statistically similar, which again proves the high

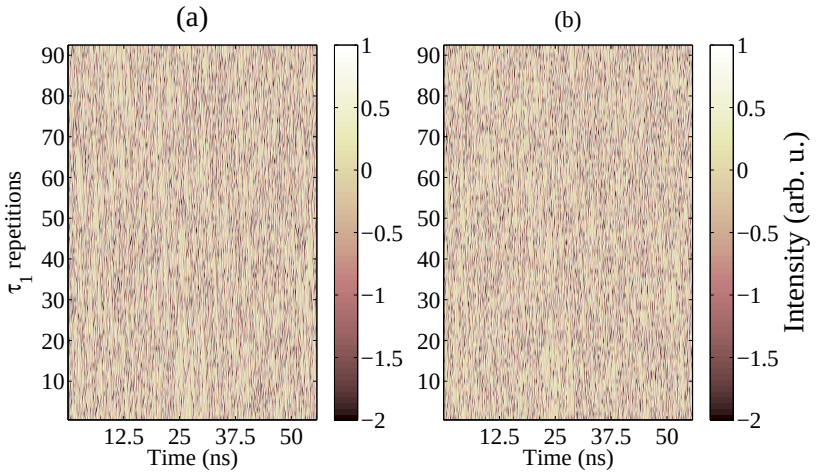

Figure 3.5: Zoom of the space-time plots of the laser output acquired at I = $1.27I_{th}$ for (a) short loop cycle, (b) long loop cycle.

quality of the replay setup.

Fig 3.6 shows a zoom of the space time plots at I = $1.27I_{th}$. Similar structures can be identified in the plots of both loops. Even though the laser received the same drive, there is not a one-to-one correspondence between figures (a) and (b). In particular, the individual structures displayed in the short loop are not captured by the long loop. Again, this is a dynamical feature not related to experimental mismatches between the loops, and means that the response of the laser to its feedback is inconsistent here. These results illustrate the ability of the laser to exhibit different and independent responses to the same drive depending on the dynamical regime, thus indicating different levels of consistency.

3.3 Quantifying consistency from experimental data

3.3.1 Consistency correlation

Consistency of the laser response is directly quantified by the cross-correlation coefficient between power output signals $x_1(t)$ and $x_2(t)$ from the short and the long loop cycle, respectively. We denote it as *consistency correlation*

$$C_c = \langle x_1(t)x_2(t)\rangle \tag{3.1}$$

where each segment is normalized such that $\langle x_i(t)\rangle = 0$ and $\langle x_i^2(t)\rangle = 1$, $i = \{1, 2\}$, and the time arguments have been deskewed by $\tau_2 - \tau_1$. Additionally to this measure, we evaluate the autocorrelation function for each of the cycles, and determine the maximum correlation of the first delay echo [92], which was used as an indicator for strong and weak chaos. We

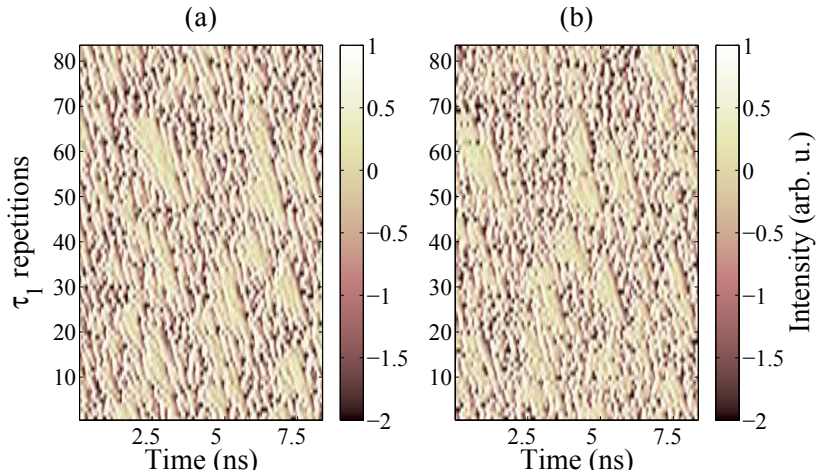

Figure 3.6: Zoom of the space-time plots of the laser output acquired at I = $1.27I_{th}$ for (a) short loop cycle, (b) long loop cycle. Figure from [86].

calculate

$$C_i = \langle x_i(t)x_i(t-t_i)\rangle, i = \{1,2\} \tag{3.2}$$

with the same normalization as above, and $t_1 \approx t_2 \approx \tau_1$ being the peak positions close to the short delay for short and long loop cycle, respectively. Figure 3.7 shows these three correlation measures as a function of the pump current.

We observe that all of the selected correlation coefficients follow the same trend by developing a single minimum at moderately low pump currents, and then rising and saturating for higher pump currents. This is a particular feature of the semiconductor laser and might not be the case for other systems. Consistency correlations up to $C_c \approx 0.99$ exemplify the high quality of the replay setup. The minimum of all correlation coefficients around $I = 13$mA indicates a possible region of strong chaos interrupting weak chaos for high and low pump currents. Despite belonging to a region of weak chaos, the correlation coefficients for low pump currents do not reach values close to one due to an insufficient signal to noise ratio. At high pump currents the values of C_1 and C_2 converge, because the signals in cycle 1 and 2 are practically identical. Around the minimum, the discrepancy between C_1 and C_2 is largest. It originates from consistency properties rather than mismatch of the drive signals. Analyzing the entire autocorrelation functions, we find that the difference is only affecting the delay echoes, whereas the zero-peak structure is identical in both cycles.

Figure 3.8 shows a detail of the autocorrelation (AC) function of the intensity dynamics for both loops obtained at $I = 1.27I_{th} = 15$mA. According to our results, this regime corresponds to an inconsistent response of the system. The resolved AC function around zero time shift is depicted in Fig. 3.8(a). The zeroth AC peaks of both loops coincide and present the same decay, in which correlations are lost after 1ns. Figure 3.8(b) shows the AC functions around the τ_1 peak. Although both delay echoes have an asymmetric shape, the signature

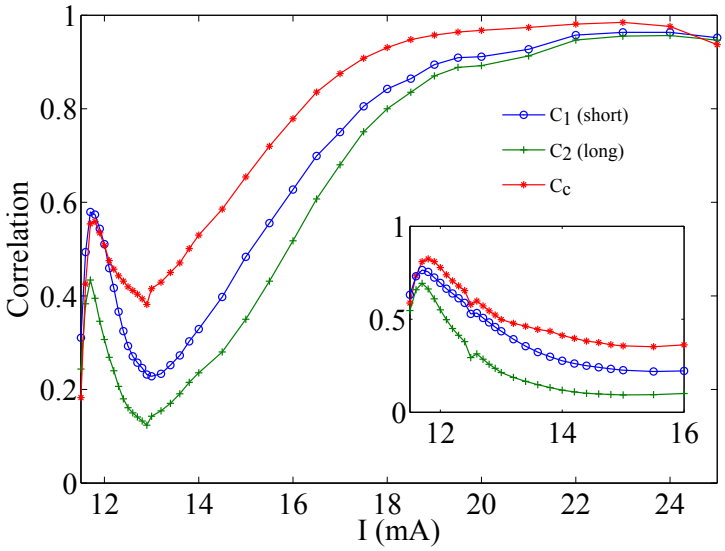

Figure 3.7: Correlation coefficients as a function of the pump current. Blue and green curves show the autocorrelation coefficients for the short and long loop cycle respectively. Red curve represents the consistency correlation. The inset shows the correlation coefficients for higher feedback strength, recorded with amplification of the detected signal. Peak positions t_1 and t_2 are depending on the pump current, and are located close to τ_1 within a margin of 50ps. Figure from [86].

from the long loop is smaller compared to the one from the short loop. The autocorrelation coefficients C_1 and C_2 are the maximum peak values of the corresponding functions in the shown range, which are close to $\tau_1 = 111$ns. In figure 3.8(b), the values of C_1 and C_2 would be different and small, corresponding to a regime of strong chaos. The difference between these signatures leads to the gap between C_1 and C_2. The correlation coefficient C_1 measures the response of the laser to its own τ-delayed signal. In contrast, C_2 measures a different relationship because, due to the inconsistency, the signal $x_2(t-\tau_1)$ is not the input underlying $x_2(t)$, but $x_1(t-\tau_1)$ which is only structurally similar, like a surrogate. The lost information is reflected in the gap between C_1 and C_2 and vanishes with increasing consistency. One could also see C_2 as an indirect indicator of strong and weak chaos.

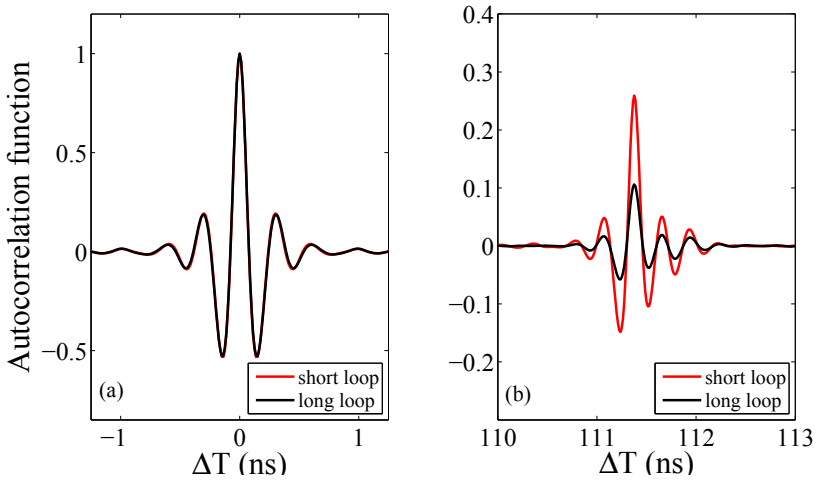

Figure 3.8: Autocorrelation function of the intensity dynamics for short loop (red) and long loop (black): (a) the resolved zeroth AC peak; (b) the resolved τ_1 peak. The curves correspond to the high feedback strength case (inset of Fig. 3.7, in which $\tau_1 = 111.42 \pm 0.05$ ns).

In order to study the transition from weak to strong chaos at low pump currents, we increased the feedback strength by almost a factor 2, changing the coupler located at the laser output for a 90/10 one. A semiconductor optical amplifier is placed in the detection path to overcome the subsequent loss in the detected signal power. The resulting correlation coefficients are shown in the inset of Fig. 3.7. The three correlation measures show a stronger increase for low and moderate pump currents with a maximum around $I = 11.8$mA. The consistency correlation at this point goes beyond $C_c > 0.8$, corroborating the region of weak chaos. For increasing pump current, the correlation functions develop again a minimum.

We have not accessed the curves for high pump currents, although we expect them to agree with the given results of the low feedback condition, so that the consistency recovers to high values. To validate the results from low and high feedback cases, we apply the rescaling procedure presented by Porte et al. [92], which allows for mapping the dynamics from one set of parameters to another. In particular, the dynamics found for a feedback strength κ at a relative pump current $p = I/I_{th}$ is equivalent to the dynamics at another feedback κ', when the current is changed according to a scaling law $(p' - 1)/(p - 1) = (\kappa'/\kappa)^2$. The collapsed curves for the different datasets of the 50/50 coupler and the 90/10 coupler to the pump current are shown in Fig. 3.9 for the consistency correlation. At low currents ($I < 12$mA), there is a difference in the maximum values of the correlation which is related to the level of measurement noise, being in the order of the small oscillation amplitudes close to the lasing threshold. Above 12mA, the two curves almost coincide with the position and the value of the local minimum agreeing as expected. Note that remaining differences can be related to the slightly varying experimental conditions and the different measurement path including an optical amplifier. Given the remarkable accuracy and range of the scaling regime, we

conclude that in an even higher feedback scheme, the same dynamical transitions would be found at correspondingly high currents.

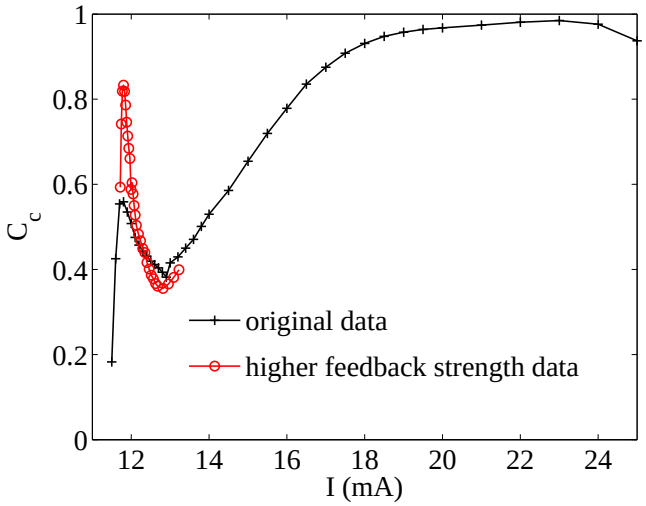

Figure 3.9: Consistency correlations as a function of pump current. Black line shows the consistency correlation for the data acquired with lower feedback strength. Red line shows the consistency correlation for the higher feedback case rescaled with a factor $(\kappa'/\kappa)^2$.

3.3.2 Sub-Lyapunov exponents from transverse distribution functions

Aside from the consistency correlation, the consistency properties can still be characterized with a more direct parameter: the sub-Lyapunov exponent. To obtain it from the experimental data is not a trivial task. Here, we present a method to extract the sub-Lyapunov exponent based on transverse distribution functions.

The transverse signal results from the substraction of signals from the short delay cycle $x_1(t)$ and the long delay cycle $x_2(t)$ deskewed $\tau_2 - \tau_1$.

$$v(t) = x_1(t) - x_2(t). \tag{3.3}$$

The term *transverse* refers to the corresponding generalized synchronization setup, in which $v(t)$ is the synchronization error, i.e., a projection of the phase space components transverse to the synchronization manifold. Thus, in case of high consistency, this transverse signal should be very close to zero. With normalization as above, the variance of the transverse signal $s_v = \langle v^2 \rangle - \langle v \rangle^2$ is directly connected to the consistency correlation by

$$C_c = 1 - \langle s_v^2 \rangle / 2 = 1 - \langle v^2 \rangle / 2. \tag{3.4}$$

However, additional information can be obtained from the distribution function of $v(t)$, where the sub-Lyapunov exponent leaves a signature. For complete synchronization of coupled dis-

crete maps, it was shown that the transverse component follows a power law distribution [53]

$$p(v) \propto |v|^{\sigma-1}. \tag{3.5}$$

Here, the transverse component is obtained from the variables, denoting the state of identical maps with discrete time. The power law exponent σ is directly related to the transverse Lyapunov exponent λ_t, such that close to the synchronization threshold holds

$$\sigma \propto \lambda_t. \tag{3.6}$$

Although for continuous systems with vector-valued state variables a complete theory is not yet developed, we show how, in analogy to the case of discrete maps, it is possible to extract a power law exponent σ which is proportional to the sub-LE λ_0. To do so, we need the linearized equations of motion close to the consistency manifold $\mathbf{x}_1(t) \approx \mathbf{x}_2(t)$ where $\mathbf{x}_1, \mathbf{x}_2$ denote the B-dimensional state vectors of the system. We stress that, with the experimental intensity time traces alone, we can only access a scalar projection of such state vectors. The system follows the set of equations of the form:

$$\begin{aligned} \dot{\mathbf{x}}_1(t) &= \mathbf{f}(\mathbf{x}_1(t)) + \kappa \mathbf{h}(\mathbf{x}_1(t-\tau_1)) \\ \dot{\mathbf{x}}_2(t) &= \mathbf{f}(\mathbf{x}_2(t) + \kappa \mathbf{h}(\mathbf{x}_1(t-\tau_1)). \end{aligned} \tag{3.7}$$

Here, $\mathbf{x}_1 \in \mathbb{R}^3$ is the state of the drive system receiving delayed feedback by a coupling function $\mathbf{h}$ with strength κ and delay τ. $\mathbf{x}_2 \in \mathbb{R}^3$ is the state of the identical response system driven by the same delayed feedback $\mathbf{x}_1(t-\tau_1)$, so that the setup supports complete synchronization. The transverse state vector is defined as

$$\mathbf{v}(t) = \mathbf{x}_1(t) - \mathbf{x}_2(t). \tag{3.8}$$

Assuming that $\mathbf{v}(t)$ describes a small perturbation governed by linearized equations of motion, the logarithm of the perturbation size, defined as

$$l_v(t) = \ln \|\mathbf{v}(t)\| \tag{3.9}$$

leads to

$$\lambda_0 = \lim_{t\to\infty} \frac{l_v(t) - l_v(0)}{t} = \langle dl_v(t)/dt \rangle_t \tag{3.10}$$

as its average growth rate. In agreement with this definition, we can write a differential equation

$$dl_v(t)/dt = \lambda_0 + \eta(t). \tag{3.11}$$

The sub-Lyapunov exponent acts as the drift term while the term $\eta(t)$ incorporates the finite time fluctuations of the Lyapunov exponent such that $\langle \eta(t) \rangle_t = 0$. Assuming the same limiting and reinjection mechanisms as in the corresponding theory for the discrete maps, we expect an exponential distribution

$$\rho(l_v) \propto \exp(\sigma l_v) \tag{3.12}$$

with

$$\sigma = \lambda_0 / D. \tag{3.13}$$

The scaling factor D is related to the intensity of the fluctuations in $\eta(t)$. If $\eta(t)$ were white noise, its spectral power density would be $2D$ accordingly. The exponential distribution is valid only in the regime governed by the linear equations of motion. For small arguments l_v the distribution is limited by noise and parameter mismatches, which in the double delay loop experiment only arise from the minimal differences between the two feedback loops. This is a major reason for the resulting high quality of the transverse signal, which allows for the analysis of the distribution function $\rho(l_v)$. For large arguments l_v, the distribution is cut off by nonlinearities because the transverse coordinate is bounded by the typical standard deviation of the trajectories.

Sub-Lyapunov exponent from experimental transverse distribution functions

To obtain the transverse distribution function from the experimental time traces $x_1(t)$ and $x_2(t)$, a reconstruction of the vector states $\mathbf{x}_1(t)$ and $\mathbf{x}_2(t)$ is necessary. We choose the canonical delay embedding [98, 99] with an embedding dimension b and an embedding delay h, such that each vector state is approximated by

$$\mathbf{x}_i(t) \sim \mathbf{y}_i(t) = (x_i(t), x_i(t-h), \ldots, x_i(t-(b-1)h))^\top, i = \{1, 2\}. \tag{3.14}$$

Although the embedding reconstruction is not guaranteed formally by Taken's theorem, because the signals originate from externally driven systems, the reconstruction error is expected to be reduced in the transverse signal because the explicit dependence on the external drive vanishes here. Thus, we calculate the logarithmic distance

$$l_v(t) = \ln \|\mathbf{y}_1(t) - \mathbf{y}_2(t)\| \tag{3.15}$$

for different values of embedding dimension and embedding delay. To corroborate these assumptions, we have numerically simulated this scheme with the Lang-Kobayashi rate equations. The analysis is shown in section 3.4.

To calculate 3.15, we reconstruct the phase space with delay embedding for a dimension $b \in \{1 \ldots 7\}$. Again, the time axis of the long loop is properly deskewed by $\tau_2 - \tau_1$. Two experimental distribution functions $\rho(l_v)$ for two different pump currents are shown on a logarithmic scale in Fig. 3.10 for embedding dimension $b = 3$. The embedding delay is chosen as the first zero-crossing of the autocorrelation function from the short loop signal. In the two figures, three regimes can be identified:

1. On the left side, the distribution is dominated by the small differences between the loops, mainly due to intrinsic noise. The scaling of this regime reveals the embedding dimension b, which agrees with the slope of the curve.

2. The regime in the middle is governed by the linear equations of motion, and presents the constant slope σ that we extract.

3. On the right side, the regime is mainly characterized by a high amplitude cutoff due to the nonlinearities of the system. This is because the difference between short and long loop is bounded by the standard deviation of the transverse signal, i.e. the size of the attractor.

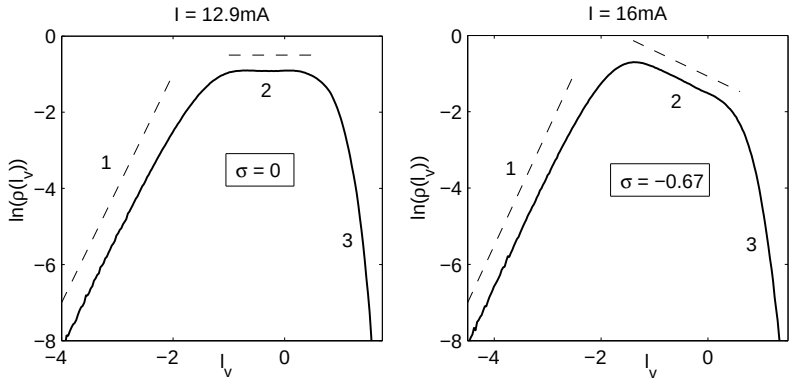

Figure 3.10: Distribution functions of the logarithmic synchronization error $l_v = \ln \|\mathbf{y}_1 - \mathbf{y}_2\|$ between short and long loop for two different pump currents revealing two different values of the slope σ. In the logarithmic plot, one can distinguish three regimes as labeled. 1) Noise-dominated. The slope agrees with the embedding dimension as indicated by the dashed line. 2) Intermediate regime governed by Lyapunov stability reveals slope σ, indicated by dashed line. 3) Cutoff regime due to boundedness of transverse component.

As shown in Fig.3.10, different operating conditions lead to different plateaus of the function $\ln(\rho(l_v))$ with slope $d\ln(\rho(l_v))/dl_v$ and consequently, different values of σ. Next, we determine the slope σ in the useful intermediate region from the set of transverse distribution functions for different embedding dimensions. For each of the time series, we extract the value of σ from the distribution function $\rho(l_v)$. The main criterion for the method is the convergence of the slope by increasing embedding dimension as illustrated in Fig. 3.11. The slope of the logarithm of the distribution function, $d(\ln(\rho(l_v)))/dl_v$, is shown for embedding dimensions $b = 2$ to $b = 7$. In the noise-dominated regime where values of l_v are small, the slope indicates the dimension. For large l_v, the fall-off corresponds to the cutoff of the distribution function. In the intermediate regime, there is a plateau in which all slopes converge. The red circle indicates the selected point for determination of σ and its uncertainity, in this example $\sigma = -0.26 \pm 0.02$. The useful plateau might reduce to a single minimum for high dimensions.

At very low or very high pump currents, the convergence becomes less clear or not detectable; thus, we assign larger tolerances from the spread between the curves or choose not to extract a σ-value for the extreme cases. The reason for the loss of clarity has again different origins depending on the case. For low pump currents, it is due to the lower signal-to-noise ratio. For high pump currents, there is intermittency between stable emission and undamped relaxation oscillations, which are persistent on timescales larger than the acquisition time.

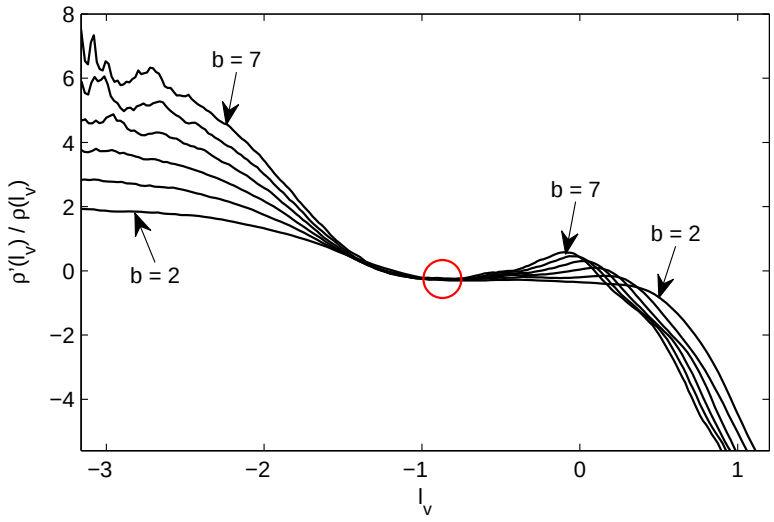

Figure 3.11: Illustration of the extraction of the value σ from the derivative of $\ln(\rho(l_v))$. Example shown for phase space reconstruction at $I = 14.5\text{mA} = 1.23I_{th}$ using the first zero-crossing of the short loop autocorrelation function as embedding delay.

The result is a multiscale transverse distribution function. Overall, the tolerances assigned to the extracted σ-values can be regarded as a procedural error. On a linear scale, the useful range for the slope extraction typically resides in the regime of 10% to 30% of the high amplitude transverse bursts.

We would like to stress that the convergence of slopes is a consequence of the power-law distribution in the transverse variable of the setup (Eq. 3.5). This distribution function is invariant under different projections and embedding dimensions. Therefore, the convergence property is a general characteristic of dynamical systems, beyond semiconductor lasers, that can be used as criterion for the σ extraction.

The main results of this analysis are summarized in Fig. 3.12, depicting the dependence of σ on the pump current. Starting with low values of σ for small currents, the curve develops a maximum coinciding with the minimum of correlations, and again decays for large currents. The values of σ over the whole range of pump current are mostly negative. We infer a large negative value of the sub-LE in the regimes of high consistency correlation, which means that intermittent bursts of the transverse variable are comparably rare, of low amplitude, and quickly recover towards periods of full consistency. The power law distribution of v with an exponent $\sigma-1$ supports this picture, as for the negative σ, there is a pronounced peak centered at $v = 0$ with a rapid decay. For intermediate pump currents, at the studied conditions, we obtain only a slight zero crossing of σ and, thus, of λ_0. Simulations indicate that this is related to the α-parameter of the employed laser, being $\alpha \sim 2$ (see section 3.4). Interestingly, a sub-LE close to zero already causes a very low consistency correlation. This shows the role of the

finite-time fluctuations $\eta(t)$ on the sub-LE which lead to large and frequent excursions from the synchronized state. In this sense, one could consider these fluctuations, which originate from intermittent desynchronization events due to noise or parameter mismatches (bubbling events) [100], as a mechanism that counteracts consistency: although the system is stable to its drive, the transverse signal presents intermittent bursts. The correspondence between Fig. 3.12 and Fig. 3.7 confirms the relationship between the sub-Lyapunov exponent and the regimes of strong and weak chaos. The pump current, at which there is the minimum of the consistency correlation, coincides with the maximum value of σ, while the minimum values of the sigma curve correspond to high values of the consistency correlation. Hence, the studies on the transverse distributions complement and extend those of the correlation functions. Recalling the direct connection between the sub-Lyapunov exponent and σ, we demonstrated the direct determination of the sub-Lyapunov exponent from experimental data. In the next section, we corroborate this relationship with numerical simulations.

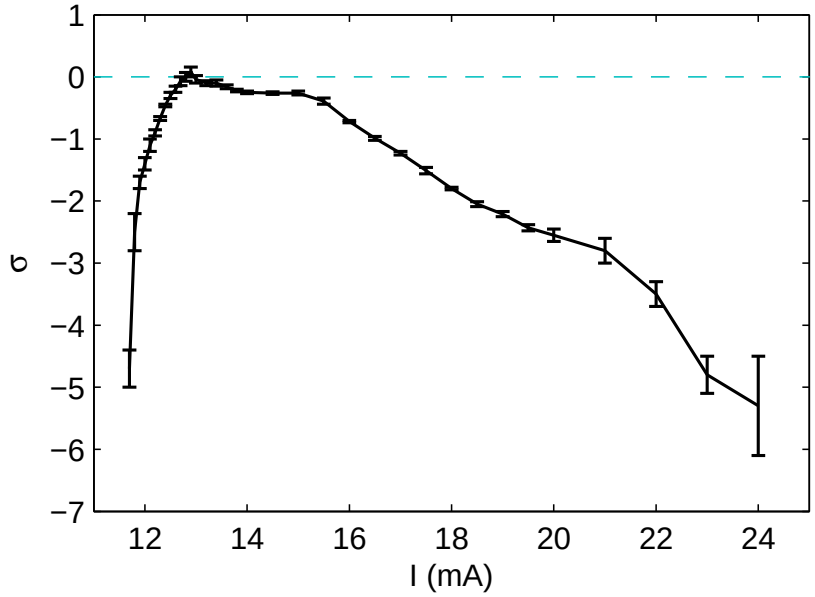

Figure 3.12: Slope $\sigma = d\ln(\rho(l_v))/dl_v$ in the intermediate regime of the transverse distribution functions. For the calculation of l_v we set the embedding delay h to the first zero-crossing of the autocorrelation function from the timetraces, and the embedding dimensions range from $b = 2$ to $b = 7$. Error bars denote the quality of convergence with increasing embedding dimension, thus, not containing systematic errors. Figure from [86].

3.4 Sub-Lyapunov exponent in numerical simulations

In order to verify our experimentally obtained results on the extraction of the slope σ, and our theoretical arguments regarding its relationship to the sub-Lyapunov exponent λ_0, we simulate a drive-response synchronization scheme with two identical units, as presented in Eq. 3.7. To introduce perturbations away from the synchronization manifold as in the realization of the experiment, we add a noise term to the equation of motion for $\dot{\mathbf{x}}_2(t)$. This noise term also allows to observe the transverse distribution function for negative sub-Lyapunov exponents by acting like a perturbation of the synchronization manifold. In comparison to the experiment, here, the state vectors of short and long loop $\mathbf{x}_1$ and $\mathbf{x}_2$ have the same time origin.

We implement the Lang-Kobayashi rate equations model [101] to simulate the dynamics of the semiconductor laser subject to delayed optical feedback. The drive and driven state contain real and imaginary parts of the complex electric field as well as the charge carrier number. The full equations for $\mathbf{x}_1 = (\Re(E_1), \Im(E_1), n_1)^\top$ and $\mathbf{x}_2 = (\Re(E_2), \Im(E_2), n_2)^\top$ read

$$\begin{aligned}
\dot{E}_1(t) &= \frac{1+i\alpha}{2} G_N n_1(t) E_1(t) + \kappa E_1(t-\tau) \\
\dot{n}_1(t) &= (p-1)\gamma N_{sol} - (\Gamma + G_N n_1(t))|E_1(t)|^2 \\
\dot{E}_2(t) &= \frac{1+i\alpha}{2} G_N n_2(t) E_2(t) + \kappa E_1(t-\tau) + \sqrt{2D}(\xi_1 + i\xi_2) \\
\dot{n}_2(t) &= (p-1)\gamma N_{sol} - (\Gamma + G_N n_2(t))|E_2(t)|^2
\end{aligned} \tag{3.16}$$

with the following parameters: the gain coefficient $G_N = 2.142 \cdot 10^{-5}\text{ns}^{-1}$, the photon decay rate $\Gamma = 357\text{ns}^{-1}$, the carriers decay rate $\gamma = 0.909\text{ns}^{-1}$, the carrier density at transparency $N_{sol} = 170.7 \cdot 10^6$, and the linewidth enhancement factor $\alpha = 2.5$. The pump current enters as $p = I/I_{th}$, and we set it to 1.94. Feedback parameters are set to $\kappa = 10\text{ns}^{-1}$ for the feedback strength and $\tau = 10\text{ns}$ for the roundtrip time, which qualitatively resembles the experimental conditions nevertheless lacking detailed parameter adjustments. The noise term is set to act only on one of the two electric field components for the study of stability properties and the time series analysis method as white noise $\boldsymbol{\xi}(t)$ with $\langle \xi_i(s)\xi_j(t)\rangle = 2D\delta(t-s)\delta_{ij}$, $i,j = \{1,2\}$, such that $\sqrt{2D\delta t} = 100$. The integration method is a stochastic Heun algorithm with step size $\delta t = 0.1\text{ps}$.

Figure 3.13 summarizes the analysis of the transverse coordinate $\mathbf{v}(t) = \mathbf{x}_1(t) - \mathbf{x}_2(t)$ analog to the experimental procedure. The first derivative of the logarithm of the transverse distribution function $\rho(l_v)$ is shown for different embedding parameters. As in the experimental transverse distributions, the left side of the curves indicate the dimensionality of the embedding, while the right side presents a cutoff of the distribution function. The middle regime presents the convergence of the slope of all distribution functions over a wide range. For the thick black curve, l_v was obtained from normalized vector components $\Re(E)$, $\Im(E)$, n. For the colored thin lines, a delay embedding was applied to the intensity time traces

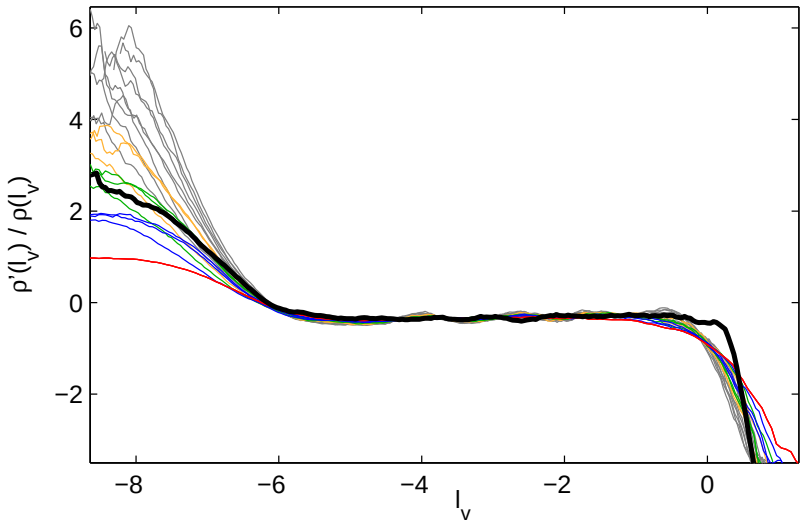

Figure 3.13: First derivative of $\ln(\rho(l_v))$ for various embedding parameters.

$P(t) = |E(t)|^2$. To achieve a match between all the plateaus, l_v from colored curves were properly shifted. The red curve corresponds to the case of no embedding $b = 1$. The rest of the curves are for embedding dimensions $b = 2$ (blue), $b = 3$ (green), $b = 4$ (orange), and $b = 5$ to $b = 7$ (gray). The multiple color curves are for various embedding delays h: $h = 0.5T_c$, $h = T_c$ and $h = 1.5T_c$ with T_c being the first zero-crossing of the short loop autocorrelation function. Due to the low noise level, we obtain a big range in which the distribution functions of $l_v = \ln \|\mathbf{v}\|$ scale with σ. The result is consistent and robust against different embedding dimensions and embedding delays applied to the time series of the intensity $P(t) = |E(t)|^2$, including even the non-embedded case of the difference signal $P_{x_1}(t) - P_{x_2}(t)$, in which false nearest neighbors appear frequently. Further, all slopes obtained by delay embedding of the intensity coincide with the slope obtained using the full vector state of $\mathbf{v}(t)$.

We also compare σ with the sub-Lyapunov exponent λ_0, which has been obtained by additionally integrating the corresponding partial linearization of the drive system in Eqs. (3.7). The plots, shown in Fig. 3.14, support a very good agreement of the curves throughout a range of α-values corresponding to the properties of the laser diodes in the experiment. For comparison of σ and λ_0, the axes are scaled by a constant factor proportional to the intensity of the finite-time fluctuations of the sub-Lyapunov exponent. Interestingly, this scaling factor emerges to be largely independent of the pump current resulting in the proportionality $\sigma \propto \lambda_0$. For $\alpha = 2.5$, a clear region of strong chaos appears where the zero-crossings of the sub-Lyapunov exponent are reproduced by σ. A lower value of the linewidth enhancement factor α leads to the avoidance of positive sub-Lyapunov exponents. From the matching between the sigma curves obtained experimentally and numerically, we can deduce that the semiconductor laser used in our experiment has a linewidth enhancement factor of $\alpha = 2.1$.

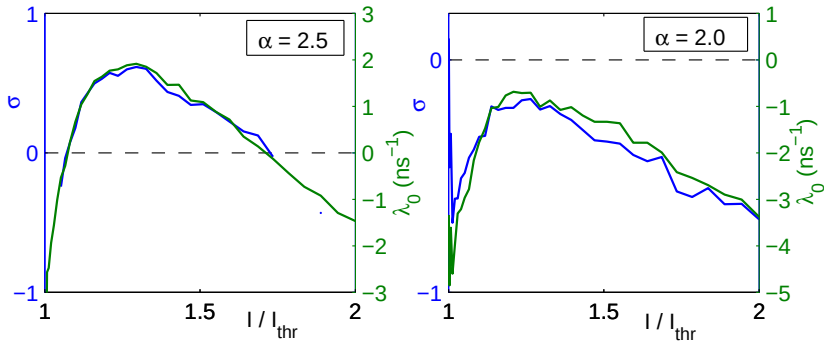

Figure 3.14: Comparison of automatically extracted value of the slope σ from distribution functions with the sub-Lyapunov exponent for $\alpha = 2.5$ (a) and $\alpha = 2$ (b). The figures show a very good agreement between σ and λ_0 with scaling factor 3ns^{-1} (a) and 5ns^{-1} (b).

This could represent a new technique to estimate the α parameter of the laser.

3.5 Summary and conclusions

We presented an optical consistency experiment based on a semiconductor laser driven by a chaotic optical signal. This chaotic drive originated from the time-delayed feedback of the laser itself, and is stored in a long fiber loop to allow for an exact repetition of the drive. The design of the experiment permits the use a non-scalar drive, in which all optical features like bandwidth, intensity or phase dynamics are kept and replayed again.

By comparing the responses of the laser, we observed that the semiconductor laser undergoes transitions from consistent to inconsistent responses and back when the pump current is increased. Such transitions are a characteristic that depends on the system employed, and other lasers may show a single transition or none at all. We relate the consistent response of the laser to a regime of weak chaos, whereas in a strong chaos regime the responses are inconsistent. We also confirmed that the consistency correlation serves as a good indicator of the different consistency regimes.

The key signature of consistency relies on the sub-Lyapunov exponent of the system, closely related to generalized synchronization. While, to date, no experimental access to the sub-Lyapunov exponent of the system existed, we have developed an experimental method to directly measure the consistency properties for high optical and dynamical bandwidth drives. By means of analysis of transverse distribution functions, we could extract σ, a direct indicator of the sub-Lyapunov exponent. The experimental method as well as the time series analysis technique are general for the synchronization of nonlinear oscillators so that, in principle, they can be applied to any type of laser or dynamical system with chaotic dynamics.

Complementary, we numerically simulated the corresponding scheme using the Lang-Kobayashi rate equations, and applied the same analysis in order to corroborate the experimental assumptions. We found consistent results for the slope σ of the distribution functions throughout all embedding dimensions and embedding delays. We further confirmed the proportionality $\sigma \propto \lambda_0$ by comparison with the directly calculated sub-Lyapunov exponent from the linear equations of motion. These findings corroborate the theoretical arguments that extend the theory for discrete maps to continuous systems, and demonstrate the robustness of the presented method. The simulations also unveil the dependence of the σ curve on the linewidth enhancement factor α, confirming consistency as a property of the laser. The good agreement between the sigma curves obtained experimentally and numerically suggest a sensitive dependence on the α factor. This phenomenon could be used to estimate the α factor or contrast its value obtained from other methods [102]. Employing the combination of experimental and theoretical methods, we provided a valuable understanding and characterization of consistency in driven systems. Given the ubiquity of "drive-response" schemes in nature, the relevance and implications of our results can be extended to dynamical systems even beyond the field of photonics.

CHAPTER 4

Consistency of a semiconductor laser system to input pulse trains

> "An approximate answer to the right problem is worth a good deal more than an exact answer to an approximate problem."
>
> John Tukey, Mathematician.

4.1 Introduction

In the previous Chapter, we introduced the concept of consistency with an experiment in which a laser system is driven by its own dynamics, playing at the same time the role of drive and response system. The external drive consisted of its own delayed feedback dynamics, exemplifying a new particular way to study the effect of complex drives on laser systems. However, this scheme can be extended to the more general case in which the input drive is an external signal, not necessarily generated from the system. In this complementary approach, an external perturbation is introduced while the laser system with feedback exhibits its own autonomous complex dynamics. The compulsory question here is: can the system under these conditions still respond consistently? If so, what are the mechanisms that lead to a consistent behavior?

Previous studies have investigated the effect of external driving on nonlinear systems [53, 83, 84, 103, 104, 105, 106, 107, 108, 109]. By means of an external drive in the form of a continuous and smooth or periodic waveforms, phenomena like stochastic resonance, synchronization or entrainment were observed [53] when the system was originally in a fixed point, periodic orbit or a limit cycle. In other cases, the drive was a chaotic signal leading to similar phenomena [52, 83]. But much less is known when a nonlinear system, operating in a complex excitable-like dynamics, is driven by non-periodic short pulses. Particularly, it is

still to be explored how the consistent response depends on the characteristics of the train of pulses, like the precise timing of a certain pulse (the temporal pattern), the average number of pulses per unit time (the pulse rate) or the amplitude of the pulses.

In this Chapter, we address the consistency properties with the laser system being in its complex chaotic regime, driven by an external train of pulses. The semiconductor laser is subject to delayed optical feedback, and operates in the regime of Low Frequency Fluctuations (LFFs). The LFF regime is characterized by a complex chaotic behavior of the light intensity on a fast timescale while, on a slow timescale, the dynamics manifest a pattern of drastic dropouts of the emitted light intensity. Studies on the effect of an external modulation to the pump current in the LFF regime have already been presented, demonstrating that a periodic drive affects the nonlinear properties of the delay system [7, 103, 104, 105, 106, 109, 110]. With our approach, we aim to investigate the feasibility of stimulating the dropouts by means of an external non-periodic pulsed drive. Different pulse distributions and pulse amplitudes are utilized to analyze the existence of optimum conditions for a consistent response. Thus, this study can be seen as a step forward in the characterization of the basic principles in the drive-response schemes with an active excitable background.

The parallelism between our approach and some aspects of the neural scenario, makes it of special interest [79, 107, 108, 111, 112, 113]. Neurons in the brain communicate with short-lasting chemical and electrical signals, processing the information in an oscillating environment which is permanently active [55, 114]. In this sense, the results presented in this Chapter allow for a better understanding of the requirements for a consistent performance under complex conditions, which in turn will allow for more efficient bio-inspired techniques of information processing like Reservoir Computing [115].

The investigations were initiated by Jordi García-Ojalvo, Javier Buldú and Ingo Fischer. The experiments and data analysis were carried out by Neus Oliver in close collaboration with Thomas Jüngling and supervised by Ingo Fischer. The simulations were carried out by Thomas Jüngling. Daniel Brunner contributed to make the pump current modulation possible.

4.2 Experimental realization

Our experimental system consists of a laser diode, subject to delayed optical feedback, and to external pump modulation in the form of electrical pulses, as depicted in Fig. 6.2. The laser is an Eblana Discrete Mode laser, lasing at 1550nm and exhibiting a threshold current of the solitary laser of I_{th}=11.8mA. It is mounted on a board that allows for modulation frequencies up to 5GHz. The LFFs regime, in which we carry the experiments, is found to be around 12.7mA. A bias-tee allows for the modulation of the pump current. The laser light is injected through non-polarization maintaining fibers into an optical circulator, which determines input and output of the fiber loop. A 50/50 optical coupler divides the passing light. 50% of the light is directly used for detection. The remaining light enters into a polarization controller

to align the polarization state of the light with respect to the laser facet. The output of the polarization controller is connected to the input of the optical circulator, thus closing the feedback loop. The round-trip time of the light in the cavity is 50ns. The DC current can be adjusted to a precision of 10μA while the temperature of the laser is controlled to a precision of 0.01K. The laser output is detected with a photodiode of 12.5GHz bandwidth, and a digital oscilloscope with 16GHz analog bandwidth. During the realization of the experiment, the low cut-off frequency of the bias-tee can cause a discharge effect when the AC drive signal is applied to the DC injection current, partly due to the high amplitude of the modulation pulses. This effect translates into small global oscillations of the baseline of the temporal waveform, which in turn can introduce some artifacts in the consistency measurements. To avoid this error, we correct the global oscillations by subtracting to the acquired time traces their sliding average, excluding the pulses. The range of the sliding average is around $400ns$.

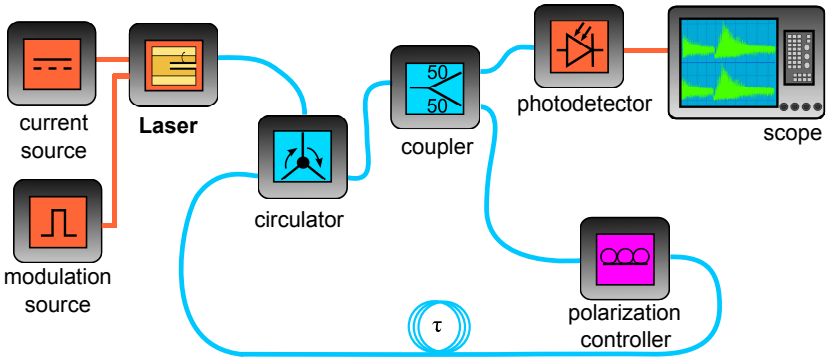

Figure 4.1: Experimental consistency setup.

When no modulation is applied, the behavior of the system corresponds to the Low Frequency Fluctuations dynamics [12, 29, 38]. This dynamical phenomenon takes place close to the solitary laser threshold, and it is characterized by cycles of a slow increase of the intensity, with fast chaotic oscillations, until a spontaneous dropout of the intensity occurs. The occurrence of the dropouts is between $400 - 900$ns, a much slower timescale than the chaotic fluctuations (typically in the sub-nanoseconds scales). Figure 4.2 illustrates a complete LFF cycle obtained from an experimental time trace. The dynamics shown are filtered to a bandwidth of 100MHz (see subsection 4.2.1). The evolution of the intensity shows fast fluctuations of the light intensity with three complete dropouts, and subsequent power-buildups phases in steps of the delay time τ.

In terms of dynamics, the LFF regime gives rise to a complex dynamical pattern with a clear timescale separation. The origin of the dropouts has been a matter of discussion and investigated from different points of view [34, 40, 41, 44, 116, 117], with a special emphasis on whether the nature of the dropouts is deterministic or stochastic [13, 40, 118, 119, 120, 121, 122]. The investigations concluded that the origin of the power drops is mainly deterministic, although noise can also influence their statistics. The mechanism leading to the LFF can be

seen as chaotic itinerancy process towards the cavity mode with the largest gain, where the trajectory gets attracted by a saddle point (anti mode) until it is repulsed back to the low gain region, causing a power drop. This chaotic itinerancy is related to the fast chaotic pulsations [43]. A look at the carrier density reveals an increase of the carriers when the dropout event takes place.

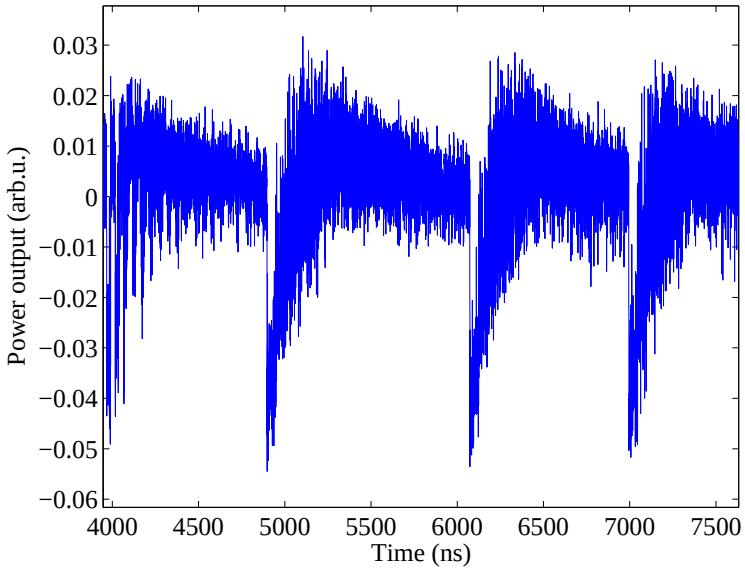

Figure 4.2: LFF cycles of a semiconductor laser with feedback obtained from experiments. The pump current was $I = 12.8$mA.

In this complex regime with excitable features, we aim to investigate the effect of an external drive with two major questions in mind: can an external stimulation induce the dropouts in a consistent manner? and what is the influence of the history of the previous dynamics? To address these questions, we inject positive electrical pulses to the laser, expecting to have an effect on the slow timescale of the system and cause a change in the carrier density like the natural dropout events do. At this point, the characteristics of the drive pulses need to be considered, such as the pulse amplitude and duration. The amplitude of the pulses is used as parameter in the following sections. For the selection of the pulse duration, we performed a qualitative investigation, in which we modulated the laser with periodic sequences of pulses, whose duration varied from 8ns to 80ns. The results showed that the duration of the pulse has a direct influence on the dropouts. A pulse too short or too long would not induce a clear dropout afterwards. In case of a triggered dropout, this would have a short duration (around 5ns) and the number of spontaneous dropouts would be more or less constant along the drive sequence, without being affected by the pulse. We observed that the best entrainment of the system was for a pulse duration between the range of 30-60ns, with slight variations. Under

such circumstance, the amount of spontaneous dropouts is significantly decreased, indicating the influence of the injected pulse in the system. These observations were in agreement with our simulations of the Lang-Kobayashi equations [101] with driving pulses:

$$\begin{aligned} \dot{E}(t) &= \frac{1+i\alpha}{2} G_N n(t) E_1(t) + \kappa E(t-\tau) \\ \dot{n}(t) &= (p(t)-1)\gamma N_{sol} - (\Gamma + G_N n(t))|E(t)|^2 \end{aligned} \tag{4.1}$$

where p(t) includes the injection of electrical pulses of constant amplitude w and duration s at a time t_p, so that:

$$p(t) = \begin{cases} p & t < t_p \\ p+w & t_p \leq t \leq t_p + s \\ p & t > t_p + s \end{cases}$$

with the following parameters: the gain coefficient $G_N = 2.142 \cdot 10^{-5}\text{ns}^{-1}$, the photon decay rate $\Gamma = 357\text{ns}^{-1}$, the carriers decay rate $\gamma = 0.909\text{ns}^{-1}$, the carrier density at transparency $N_{sol} = 170.7 \cdot 10^6$ and the linewidth enhancement factor $\alpha = 5$. The pump current p is defined as $p = I/I_{th}$ and set to 1.02. Feedback parameters are $\kappa = 100\text{ns}^{-1}$ for the feedback strength and $\tau = 10$ns for the roundtrip time. The duration of the LFF cycle is 250ns. With these simulations, we aim to explore qualitatively the effect of an external pulse within the LFF cycle, so that the parameter values do not necessarily coincide with the values of the laser used in the experiment. A pulse induced dropout is depicted in Fig. 4.3 for a pulse amplitude of 14mV (or 0.4mA) and duration s of 10ns. In blue, the evolution of the intensity dynamics filtered to a bandwidth of 100MHz is displayed. The green curve represents the time at which the modulation pulse was injected (around 175ns), but also the adiabatic solitary emission intensity. The simulations show that the pulse induces a dropout, although it is not as pronounced as the spontaneous one taking place at 280ns. The duration of the pulse was varied in an analogous way to our experimental observations, exhibiting the best entrainment for a pulse duration equal to the delay time of the system.

To examine the possibility of pulse-induced dropouts experimentally, two different pulse distributions are used to modulate the pump current: a bimodal distribution and a uniform distribution of pulses. With the bimodal distribution, we attempt to study the existence of a sensitive and insensitive phase of the LFF cycle after the pulse as well as its dependence on the past pulses. With the uniform distribution, we aim to investigate the effect of the spacing between pulses when randomly varied following a uniform distribution. In both cases, the pulses have the same duration as the delay time of the system. This method requires a new interpretation of consistency. Now, the evaluation of a consistent or inconsistent response is confined to the dynamical features of the response system in a given time window after every pulse and throughout the replay of every train of pulses. Besides, this operation permits the distinction between inter- and intra-correlations, thus gaining a deeper insight into the conditions for a consistent and yet complex temporal behavior.

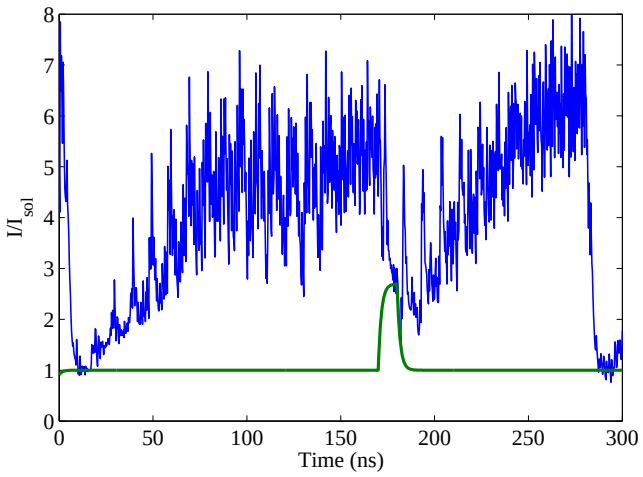

Figure 4.3: Typical LFF cycle of a semiconductor laser with feedback obtained from numerical simulations. A pulse of 14mV was introduced after 175ns.

4.2.1 A study at slow timescales

The regime of Low Frequency Fluctuations, as described in the previous section, has a slow and fast dynamics. The LFF cycle, as the power dropout and the power-buildup, is repeated in the slower timescale. To facilitate the recognition of global features of the responses to the perturbations in the LFF cycles, the fast frequency components have been filtered out. Thus, a pre-filtering to the recorded time traces is applied. Figure 4.4 (a) shows the laser response to modulation of pulses with a bandwidth of 1GHz, as acquired from the oscilloscope. Figure 4.4 (b) shows the same responses with a reduced bandwidth of 100MHz. The intensity dropouts are hidden within the fast oscillations of the system when the bandwidth is 1GHz. After the filtering, the dropouts are easier to identify and the characteristics of the individual responses, such as the depth of the dropout or the slope of the recovery, can be better compared. An extended study on the effect of filtering in the consistency of responses is presented in section 4.5.

4.3 Influence of the history of pulses: injecting a bimodal distribution of pulses

In this section, we examine two different aspects of consistency: the influence of the pulse position within the LFF cycle and the influence of the history of previous pulses. The designed train of pulses follows a bimodal distribution, so that the interval between two consecutive pulses has two possible values, each with a 50% of probability. One of the times is adjusted

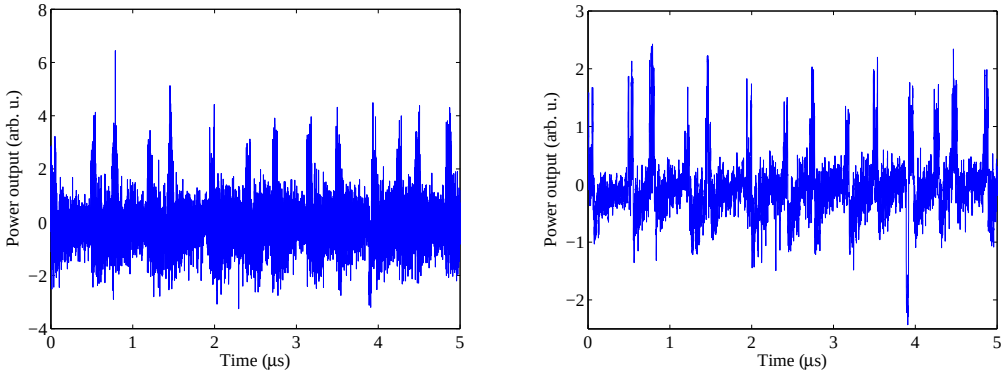

(a) (b)

Figure 4.4: Temporal waveform of the response to input pulse trains. The amplitude of the modulation pulses was set to 25mV.

to the typical inter-dropout time of the autonomous dynamics, propitious for the stimulation of a dropout, while the other time interval is shorter and, in principle, not favorable for the pulse to induce a dropout. The bimodal modulation comprises pulses of 50ns of duration to match the delay time of the fiber loop. The pulse amplitude is initially set to 25mV, which in terms of pump current is equivalent to +1mA. Later in the study, the amplitude of the pulses is changed and used as parameter. Figure 4.5 shows the first 25μs of the bimodal modulation sequence, which has a total duration of 100μs. The number of pulses contained in the train is 281.

Many features of the responses are nicely represented in persistence plots. A persistence plot is an ensemble of time traces plotted as a density plot and averaged over a certain time, 20s in our case. This is a very powerful experimental tool, since it allows to visualize up to 2.000 responses at the same time in a fast and intuitive way. Such plots can be captured directly via the oscilloscope. In order to obtain the same amount of information from numerical simulations, long computational times would be required. An example with the response of the laser to bimodal modulation is shown in Figure 4.6. The vertical axis represents the light intensity as the photodiode voltage output. The horizontal axis represents the time, 500ns per division. The color codes the frequency of the trajectory occurring at certain time-intensity coordinates, so that white means no occurrence and red means maximum frequency. Fig. 4.6 was obtained with a sampling rate of 10 GSamples/s and a bandwidth of 1GHz. To have it stabilized in time, we used a marker in the modulation sequence as a trigger. The persistence plot can be understood as a way to visualize the inter-correlation.

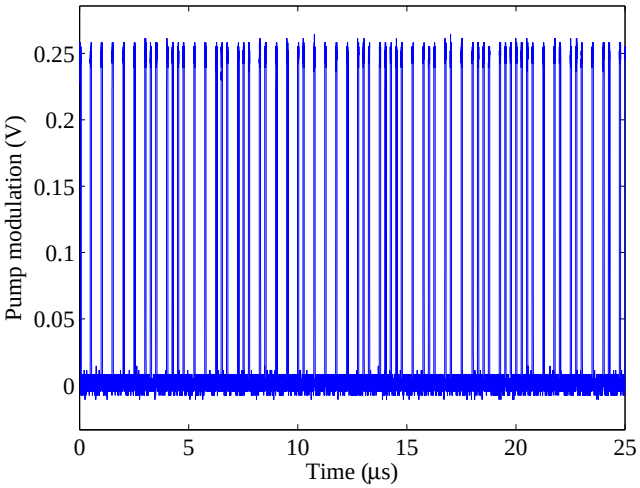

Figure 4.5: First 25μs of the bimodal input pulse train affecting the pump current of the laser system. The total duration of the modulation sequence is 100μs.

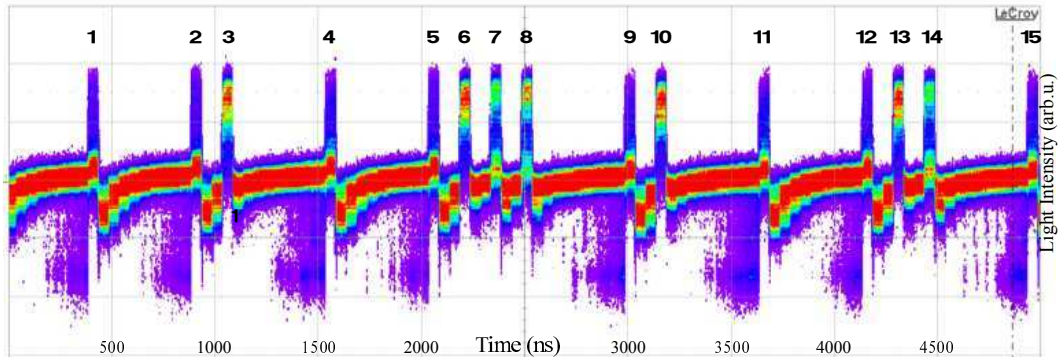

Figure 4.6: Persistence plot of the response of the laser to a bimodal modulation sequence. In this case, the two allowed interval between pulses where 150ns or 500ns. The pulse amplitude is 25mV.

In Fig. 4.6, 15 different pulse responses can be identified. The position and duration of the pulses is captured in the persistence plot as a short and relatively high elevation of the intensity from the mean. Besides, spontaneous dropouts are also identifiable. The spontaneous dropouts take place typically before the incidence of a pulse, and are represented as a lowering of the intensity with an amplitude comparable to the injected pulse's amplitude. In the figure, they show up in purple color. Remarkably, the induced dropouts are less profound than the natural ones, as observed in the simulations of Fig. 4.3.

Analyzing the responses to the perturbations in a bimodal distribution, we can classify

them into two. On the one hand, there are pulses capable to trigger a dropout after the pulse. It is the case for pulse responses 1, 2, 4, 5, 7, 9, 11, 12 and 14 of Fig. 4.6. On the other hand, there are responses that do not have a significant effect on the intensity after the pulse, but cause an elevation of the intensity during the pulse itself. This corresponds to responses of pulses 3, 6, 8, 10 and 13. We can extract from Fig. 4.6 that, although the responses are different from one pulse to another, the response to a certain pulse of the modulation sequence is consistent. In other words, responses have a higher inter-correlation than an intra-correlation.

A reason for this difference between inter- and intra-responses lies on the effect of history in the pulse responses. For instance, pulses 4 and 11 have a similar history: before each pulse there is an interval of 500ns, two pulses spaced 150ns and an another interval of 500ns. The average of responses for the two pulses is very similar since both pulses trigger a dropout consistently. If we now compare the responses to the 8th pulse and to the 14th pulse, we see that they also have a previous history in common: before the reference pulse comes a blank interval of 150ns, preceded by a pulse (7th/13th), another 150ns interval and another pulse(6th/12th). However, their responses are slightly different. Responses to the 14th seem to trigger more dropouts, whereas the responses to pulse 8th consist of an elevation of the intensity during the pulse. This can only be due to the difference between the precedents of the 6th and 12th pulse, meaning that history beyond 400ns still plays a role in the responses.

To further quantify the observations from the persistence plot, we performed the inter- and intra- correlation calculations.

4.3.1 Consistency for a bimodal distribution of drive pulses

We calculate both inter-correlation (pairs of responses only belonging to the same pulse in the sequence) and intra-correlation (pairs of responses from different pulses along the sequence) using the same global normalization procedure as introduced in Chapter 2. The analysis is intended to clarify the impact of a given pulse in the efficient stimulation of a dropout. While the intra-correlation compares the responses to all the pulses of the sequence, some of which trigger a dropout consistently and some of which do not, the inter-correlation compares the responses to a certain pulse of the drive train within the different repetitions.

For the computation of correlations, we perform 88 repetitions of the modulation sequence. The inter-pulse times have two possible values: 190ns and 500ns. The window for the calculation of the inter- and intra- correlations begins right after the pulse, so that the calculation of the correlation includes only the response of the system to the pulse, excluding the elevation of the dynamics during the pulse itself that could lead to false higher correlation values.

The pulse amplitude was varied between 8mV and 250mV. An example of the effect of the pulse amplitude on the responses can be seen from Figure 4.7. The ensemble of the 88 responses to the modulation is represented in grey, whereas, in blue, only one trial is highlighted. This visual comparison between a given trial and the whole ensemble is the basis of the calculations based on ensemble correlations. In Fig. 4.7(a), the pulse amplitude

is 25mV, whereas in Fig. 4.7 (b), the amplitude of the pulse was 79mV.

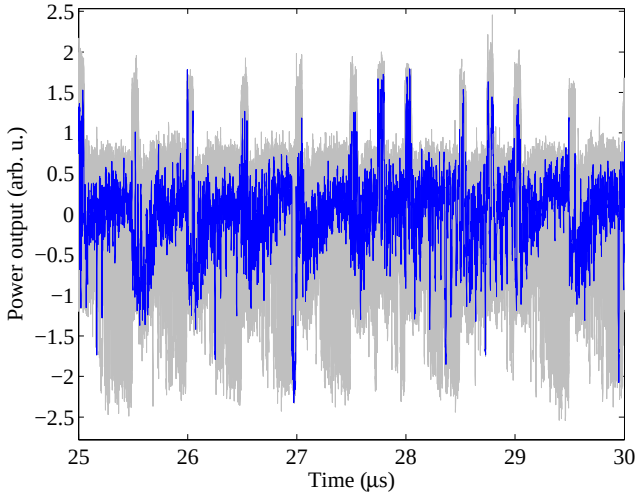

(a)

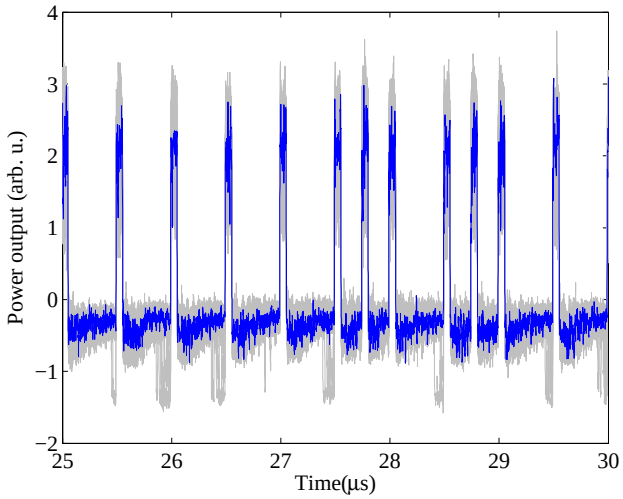

(b)

Figure 4.7: Temporal waveforms of the response to input pulse trains. The amplitude of the modulation pulses was set to (a) 25mV and (b) 79mV.

In both figures, the signatures of the pulses can be identified in the time traces, demonstrating that the two drives, comprising different amplitude pulse trains, affect the dynamics. The variability in dynamical responses seems larger for smaller amplitudes of the pulse, whereas for higher values of pulse amplitude, the responses are more confined. It is worth

noticing that the amount of spontaneous dropouts taking place before the occurrence of a pulse is significantly smaller when the pulse amplitude is big. The depth of the power-dropout is also slightly reduced when the amplitude of the pulses is 79mV.

The result of the correlation determination as a function of the pulse amplitude is shown in Figure 4.8. The curves for inter- and intra- correlation show the same trend, with an overall increase of the correlation with the pulse amplitude. For all pulse amplitudes, the correlation between responses is always higher for inter-trials than for the intra-trials, exhibiting for some amplitudes a percentage difference of up to 86%. This result agrees with the contrast observed in the persistence plot. Small pulse amplitude are non-invasive, having a non apparent influence on the dynamics. Pulses with amplitudes above the 200mV tend to control the autonomous dynamics, which reacts in a similar way to any perturbation. A local maximum around pulses of 25mV amplitude appears in Fig. 4.8. This nontrivial extremum could be due to the perfect match between the height of the pulses and the average depth of the power dropouts induced. The global increase in correlation with the pulse amplitude can also indicate that the fast degrees of freedom become more consistent as the pulse grows, not acting as additive uncorrelated noise anymore.

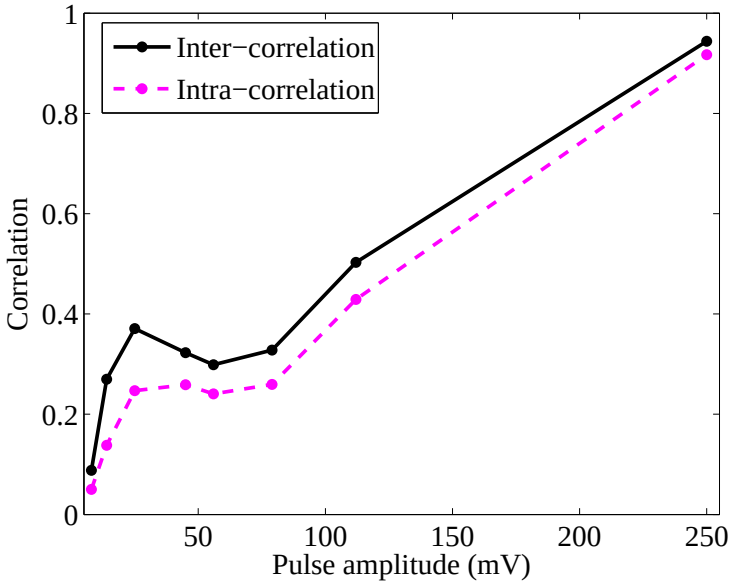

Figure 4.8: Comparison of the inter- and intra-correlation values as a function of the pulse amplitude for a modulation sequence with pulses spaced either 190ns or 500ns.

4.4

Influence of the inter-pulse intervals: injecting a uniform distribution of pulses

Another important parameter to investigate is the inter-pulse interval. To fully characterize the consistency properties, it is mandatory to know whether the time between pulses is a crucial control parameter, and how does the interval time affect the responses. We address these points by repeating the same study as described above with a pulse sequence following a uniform distribution. Now, the drive sequence consists of pulses of 50ns randomly spaced, with intervals ranging from 200ns to 500ns. The amplitude of the pulses is again varied in the study from 8mV to 250mV. The modulation sequence is depicted up to 25μs in Figure 4.9.

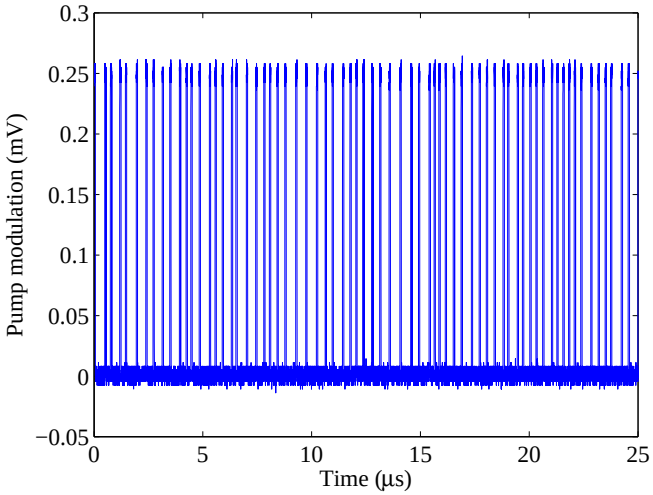

Figure 4.9: First 25μs of the uniform input pulse train affecting the pump current of the laser system. The total duration of the modulation sequence is 100μs.

The persistence plot of the time traces with modulation by a uniformly distributed pulse train is shown in Fig. 4.10. Again, the persistence mode of the oscilloscope was enabled for 20s, so that 2000 time traces are superimposed. The vertical and horizontal axes represent the light intensity and the time, respectively, while the color scale represents the probability density, from no occurrence (white) to maximum density (red). The sampling rate of the scope during the acquisition of Fig. 4.10 was 10GSamples/s with a bandwidth of 1GHz.

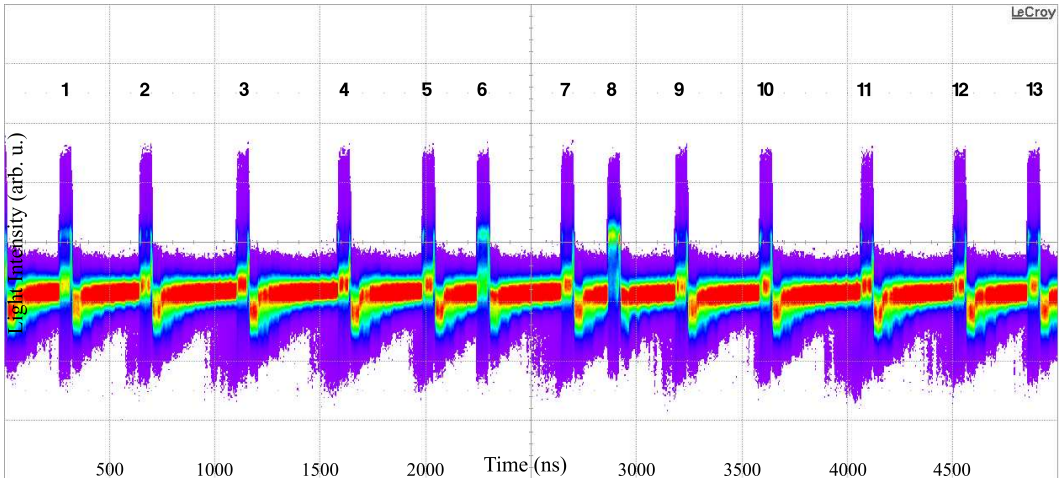

Figure 4.10: Persistence plot of the response of the laser to a uniformly distributed modulation. The pulse amplitude is 25mV.

13 pulses can be distinguished in Fig. 4.10. In contrast to the bimodal distribution of pulses, here, the responses cannot be categorized into only two types. Due to the variability of the inter-pulse times, the responses to the pulses also cover a broader range, from inconsistent to consistent response. If we look at the response to the third pulse, it shows a high degree of consistency in triggering a dropout. So does the response to the 8th pulse, which presents consistency in another behavior: the elevation of the intensity. However, the responses to the pulses 2, 4, 9 are more difficult to classify. The pulses are capable to induce a dropout, but not in a systematic manner. These are the pulses with an inconsistent response, since the outcome varies with every repetition of the sequence.

As a general observation, the inter-pulse time plays a role in the type of response. If the interval between consecutive pulses is too short, the second pulse will not lead to a dropout, but the intensity dynamics would be transiently elevated during the pulse itself. A too large interval is not favorable either, since the dropouts can then occur spontaneously. To induce a dropout, the time interval should be chosen approximately equal to the duration of a natural LFFs cycle.

4.4.1 Consistency for a uniform distribution of drive pulses

Comparatively to the study of consistency in section 4.3.1, we perform the calculations of the inter-correlation and intra-correlation for the modulation sequence following a uniform distribution of pulses (for a more detailed information see Chapter 1). The window used for the calculation has a duration of 100ns, excluding the pulse and limited by the shortest time interval.

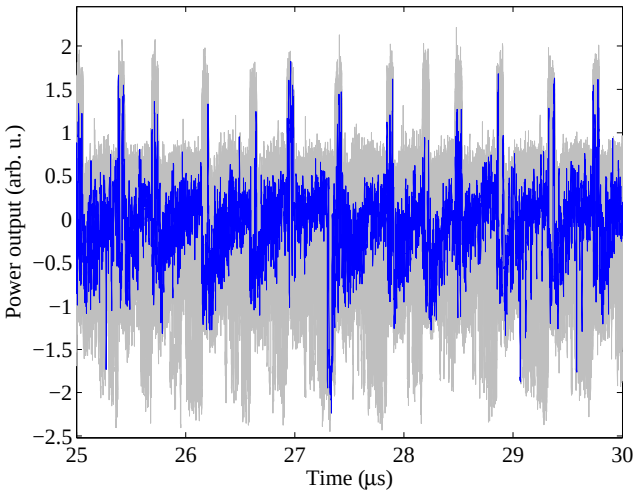

(a)

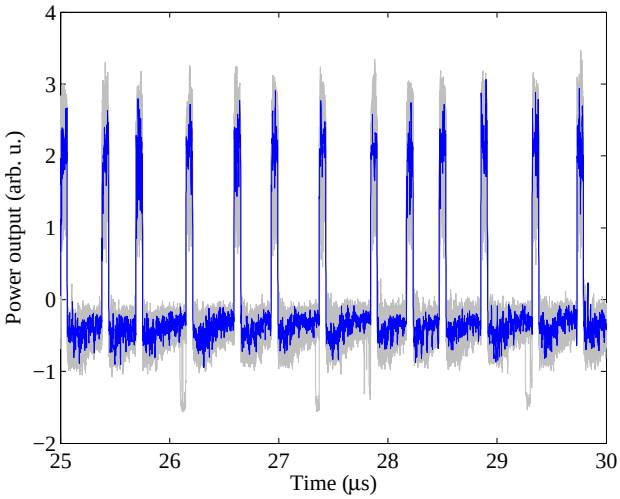

(b)

Figure 4.11: Temporal waveform of the response to input pulse trains following a uniform distribution. The grey color represents the ensemble of trajectories. The blue color highlights a response randomly selected. The amplitude of the modulation pulses was set to (a) 25mV and (b) 79mV.

As in the case of pulse train following the bimodal distribution, the amplitude of the pulse has a dramatic effect on the dynamics. In figure 4.11, we present the ensemble of the responses in grey with a given trial in blue for a pulse amplitude of (a) 25mV and (b) 79mV. Again, the differences in the type of responses between the two amplitudes are noticeable.

Even though the train of pulses is the same for both amplitudes, the case of Fig. 4.11 (b) is characterized by a strong reduction in the number of spontaneous dropouts prior to a pulse as compared with Fig. 4.11 (a). The profundity of the spontaneous power-drops is also decreased for Fig. 4.11 (b). The ensemble of all time traces reduces its range of oscillations as the input amplitude increases, reducing the difference between the single time trace and the ensemble.

Figure 4.12 depicts the correlations as a function of the pulse amplitude. The correlation values for inter- and intra- correlation increase with the pulse amplitude, showing the same tendency as for the bimodal distribution. Again, the inter-correlation is higher than the intra-correlation for all pulse amplitudes, although the contrast between them is in average smaller than in the bimodal case. The reason is due to the inconsistency of the responses to certain pulses. If a given pulse of the sequence is not capable to induce the same behavior in every repetition, the ensemble of inter-responses will be more similar to the ensemble of intra-responses, where all the experimental dynamical responses are captured. The low correlation values at small amplitudes indicate that the pulses are too small to have any impact. The amplitude of 25mV also presents a relative extreme in the correlation, proving its origin is not related to the type of modulation. The inter-correlation and intra-correlation display a plateau between 50mV and 79mV, after which the correlation values increase and become more similar.

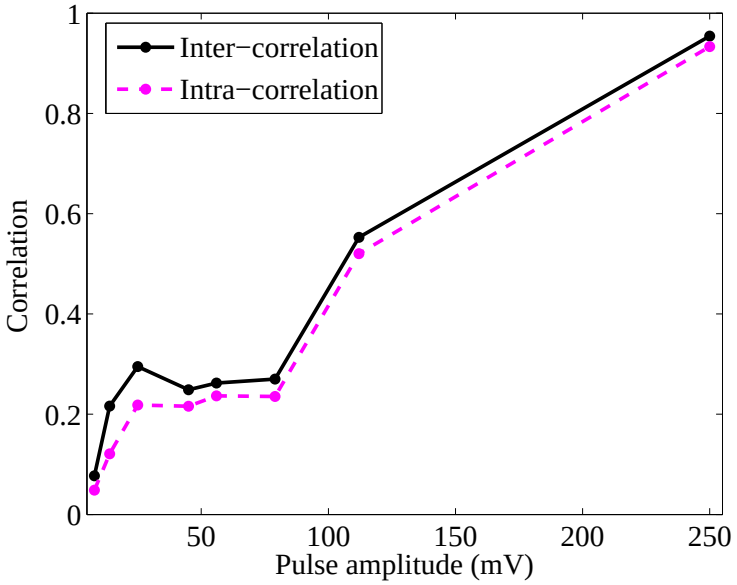

Figure 4.12: Comparison of the inter- and intra-correlation values as a function of the pulse amplitude for a modulation sequence with pulses uniformly spaced in the range [200, 500]ns.

4.5 Filtering the responses

In the previous sections, we filtered the recorded time traces to a 100MHz bandwidth. In this section, we study the effect of the bandwidth on the correlation values by varying the normalized cutoff frequency of a 2nd-order low-pass digital Butterworth filter from 20MHz to 500MHz. The different correlation values as a function of the pulse amplitude can be seen in Figure 4.13 (a) for the bimodal distribution and (b) for the uniform distribution. Interestingly, both distributions show the same trend for the different filter bandwidths. In all the presented cases, the inter-correlation is greater than the intra-correlation. The contrast between inter-correlation and intra-correlation is moderately reduced when the distribution of drive pulses is uniform. For a bandwidth of 50MHz or smaller, the local maximum around 25mV vanishes, indicating the loss of intrinsic dynamical features, and the two correlations converge for all the pulse amplitudes studied. Filtering the responses to a bandwidth of 200Mz or above causes the reduction of the contrast between inter- and intra-correlations, particularly at small pulse amplitudes. This shows that the power dropouts are less distinguishable among the fast oscillations of the dynamics. Since we are interested in preserving as many original features of the dynamics as possible, and, at the same time, we want to highlight the difference between the inter- and intra-correlations, the best compromise seems to be a filtering of 100MHz.

There is an increase of correlation values when decreasing the cutoff frequency for all the pulse amplitudes considered. This tendency suggests that the overall low correlation values can be caused by uncorrelated high-frequency components of the signal and, the more we filter, the more the uncorrelated frequencies are excluded. This effect is, however, minor for high pulse amplitudes, which indicates that the amplitude of the pulse is so large that it enslaves the system, including the high frequency components.

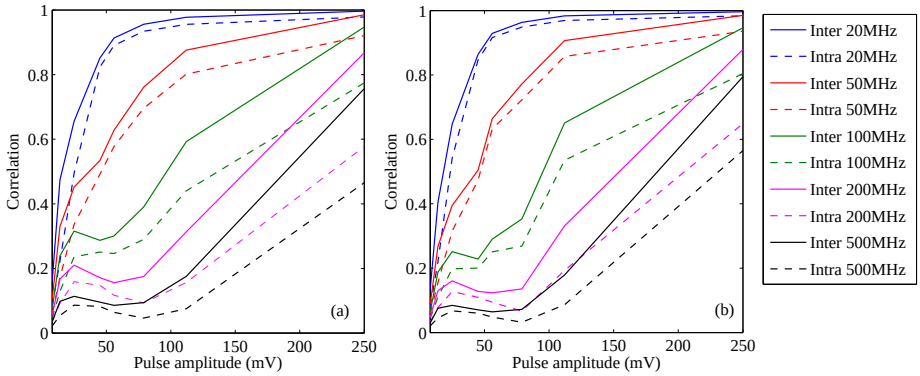

Figure 4.13: Inter- and intra-correlations as a function of the pulse amplitude for different filtering bandwidths. (a) Using a bimodal distribution of pulses as drive. (b) Using a uniform distribution of pulses as drive. Inter-correlations are plotted with solid lines, whereas intra-correlations are plotted with dashed lines. Every color represents a cutoff frequency.

4.6 Summary and conclusions

We have investigated the influence of an external drive on a semiconductor laser diode subject to optical delayed feedback. While the laser system was operating at the chaotic regime of Low Frequency Fluctuations (LFFs), we have driven the laser with two different trains of pulses, one in which the pulses followed a bimodal distribution, and one in which the pulses were uniformly distributed. Our results show that, despite its chaotic autonomous dynamics, the laser system responds in a consistent manner to the pulsed drives, reacting in a similar way when the same sequence of input trains is repeated (high inter-correlation). Nevertheless, the responses to each individual pulse of the modulation sequences maintain their own characteristics, being less similar when compared among them (low intra-correlation). We introduced new test methods to quantify consistency, such as inter- and intra-correlations, conceived for an external pulse-shaped drive. Our results unveil the importance of the temporal pulse pattern as a mechanism that can determine the consistent or inconsistent response of the system.

We have found common features between the consistency properties achieved with the two studied distribution of pulses. One of our main conclusions is that the pulse position within the modulation sequence affects the consistency of the responses. This observation is particularly noticeable in the example of the bimodal modulation train, in which consecutive pulses with a short inter-pulse time are less likely to induce a dropout, whereas pulses occurring after an interval time of 500ns tend to trigger a dropout more efficiently. However, the analysis becomes more complex if we go beyond the previous pulse, and include $n > 2$ previous pulses to the study, displaying a clear dependence of the history of the perturbation.. When the train of pulses is uniformly distributed, the range of responses is richer, reducing the contrast between the inter- and intra-correlations.

The experiments have also corroborated the existence of an optimum range of the pulse amplitude in both trains, so that the system is capable of reacting to the perturbation without being enslaved. In general terms, a range of moderate parametrical modulation amplitudes exists, in which the system shows excitability-like properties with rich dynamical features. In this range of amplitudes, the laser system can respond in a consistent manner to the pulsed drive, regardless of the complex dynamics. When the pulses are small, the effect on the dynamics is not perceptible, and it is probably hidden by noise. For large amplitude of pulses, the depth of the triggered dropouts is significantly reduced. As the amplitude of the pulses increases further, the responses of the laser tend to be more uniform or similar, until the distribution of the pulses (or their history) does not play a role anymore. The laser is then completely driven by the pulses, and reacts exactly the same way to them. These features are common to the two studied distribution of pulses. Whether the responses for the higher modulation amplitudes have also a high degree of consistency, so that the fast dynamics are also correlated, it is not yet clear.

Still, the research on consistency properties of nonlinear systems is far from complete.

All our results were obtained for pulsed drives, and the consistency properties for other modulation waveforms might provide other unexpected findings. Future work on responses to external drives might also concentrate on the investigation of consistency properties in other frequency domains, and with other forms of perturbations, like negative pulses. It should be noticed that our study is limited to a certain frequency band, and the equivalent discussion at fast time scales is not complete. The effect of the pulse duration is also a parameter to be explored in more detail. In our qualitative study, we observed that the duration of the pulse influences the induction of the power-dropouts. If the pulse is too short, it cannot provoke a clear dropout afterwards, and the probability of having an induced dropout after the occurrence of the pulse is similar to the probability of having an spontaneous dropout along the whole sequence. When the pulses have a too long duration, the response of the laser to different input train pulses is equivalent to having a short duration-pulse and the inter-correlation values are not necessarily higher. The best entrainment of the system was for a pulse duration between the range of 30-60ns, with slight variations. In that case, the amount of spontaneous dropouts is significantly decreased, proving the influence of the pulse in the system, and this fact also leads to higher inter-correlation values. Therefore, we set the width of the pulse to the delay time, aiming at short pulses, so they resemble an intense perturbation, spike-like, but still long enough to trigger dropouts. However, that is not a strict condition, and other pulse durations and even other time scales, like the relaxation time of the system, can be considered as an interesting option.

Our analysis complements the investigation of the fundamental drive-response relations presented in the previous Chapter, with the distinctive feature of introducing non-periodic pulsed perturbations as external drive. This work represents a study devoted to characterizing the response of a chaotic laser system, with a trustworthy imitation of neural dynamics at slow time scales. The presented results are therefore relevant for neuro-inspired information processing, given that, as a novelty, the system is in a complex excitable operating regime, with two timescales involved. We believe this work contributes to filling the existing gap on the conditions leading to induced consistency through pulses in dynamical systems. From a more applied point of view, the similarity of our scheme with the neural phenomenology might help to extend the state of the art bio-inspired information-processing concepts.